

Ultramassive dense early-type galaxies: velocity dispersion and number density evolution since $z=1.6$

A. Gargiulo^{1*}, P. Saracco², S. Tamburri^{2,3}, I. Lonoce^{2,3}, F. Ciocca^{2,3}

¹ INAF – Istituto di Astrofisica Spaziale e Fisica Cosmica Milano, via Bassini 15, 20133 Milano, Italy

² INAF - Osservatorio Astronomico di Brera, Via Brera 28, 20121 Milano, Italy

³ Dipartimento di Scienza e Alta Tecnologia, Università degli Studi dell'Insubria, via Valleggio 11, 22100 Como, Italy

Received 2015 May 20; accepted 2016 May 4

ABSTRACT

Aims. In this paper we investigate the stellar mass assembly history of ultramassive ($M_{\star} \gtrsim 10^{11} M_{\odot}$) dense ($\Sigma = M_{\star}/2\pi R_e^2 > 2500 M_{\odot} \text{pc}^{-2}$) early-type galaxies (ETGs, elliptical and spheroidal galaxies visually selected) over the last 9 Gyr.

Methods. We have traced the evolution of the comoving number density ρ of ultramassive dense ETGs and have compared their structural (effective radius R_e and stellar mass M_{\star}) and dynamical (velocity dispersion σ_e) parameters over the redshift range $0 < z < 1.6$. We have derived the number density ρ at $1.6 < z < 1$ from the MUNICS and GOODS-South surveys, while we have taken advantage of the COSMOS spectroscopic survey to probe the intermediate redshift range [0.2 - 1.0]. The number density of ultramassive dense local ETGs has been derived from the SDSS sample taking into account all the selection bias affecting the spectroscopic sample. For the comparison of the dynamical and structural parameters, we have collected a sample of 11 ultramassive dense ETGs at $1.2 < z < 1.6$ for which velocity dispersion measurements are available. For 4 of them (plus one at $z = 1.91$) we present previously unpublished estimates of velocity dispersion, based on optical VLT-FORS2 spectra. We probe the intermediate redshift range ($0.2 \lesssim z \lesssim 0.9$) using the sample of ETGs by Saglia et al. (2010), and Zahid et al. (2015) and the local universe using the sample of ETGs by Thomas et al. (2010)

Results. We find that the comoving number density of ultramassive dense ETGs evolves with z as $\rho(z) \propto (1+z)^{0.3 \pm 0.8}$ implying a decrease of $\sim 25\%$ of the population of ultramassive dense ETGs since $z = 1.6$. By comparing in the $[R_e, M_{\star}, \sigma_e]$ plane the structural and dynamical properties of high- z ultramassive dense ETGs over the range $0 \lesssim z < 1.6$ we find that all the ETGs of the high- z sample have a counterpart with similar properties in the local universe. This implies either that the majority ($\sim 70\%$) of ultramassive dense ETGs has already completed its assembly and its shaping at $\langle z \rangle = 1.4$, or that, if a significant fraction of them evolves in size, new ultramassive dense ETGs must form at $z < 1.5$ to maintain their number density almost constant. The difficulty into identify good progenitors for these new dense ETGs at $z \lesssim 1.5$, and the stellar populations properties of local ultramassive dense ETGs point toward the first hypothesis. In this case, the ultramassive dense galaxies missing in local universe can have joined, in the last 9 Gyr, the “non dense” ETGs population through minor mergers, thus contributing to mean size growth. In any case, the comparison between their number density and the number density of the whole population of ultramassive ETGs relegates their contribution to the mean size evolution to a secondary process.

Key words. galaxies: elliptical and lenticular, cD; galaxies: formation; galaxies: evolution; galaxies: high redshift

1. Introduction

Most of the studies focusing on the structural parameters of massive passive galaxies both at high and at low redshift show that this population of galaxies has increased the mean effective radius over the cosmic time (e.g. Daddi et al. 2005; Trujillo et al. 2006, 2007; Longhetti et al. 2007; Zirm et al. 2007; Toft et al. 2007; van Dokkum et al. 2008; Franx et al. 2008; Cimatti et al. 2008; Buitrago et al. 2008; van der Wel et al. 2008; Bernardi 2009; Damjanov et al. 2009; Bezanson et al. 2009; Mancini et al. 2009, 2010; Cassata et al. 2011; Damjanov et al. 2011; Bruce et al. 2012; Szomoru et al. 2012; Newman et al. 2012; Cassata et al. 2013; van der Wel et al. 2014; Belli et al. 2014). For example, van der Wel et al. (2014) find that the mean effective radius $\langle R_e \rangle$ of passive galaxies selected with a colour-colour criterion increases as $\langle R_e \rangle \propto (1+z)^{-1.48}$ over the redshift

range $0 < z < 3$. Similar results, among the others, have been reached also by Cassata et al. (2013), on samples of passive (specific star formation rate $s\text{SFR} < 10^{-11} \text{ yr}^{-1}$) galaxies, and by Cimatti et al. (2012) for galaxies with red colours and elliptical morphology. Nonetheless, other analysis contrast these results showing a mild or an even negligible evolution of the mean size with cosmic time (Saracco et al. 2011; Stott et al. 2011; Jorgensen & Chiboucas 2013; Saracco et al. 2014; Jorgensen et al. 2014; Poggianti et al. 2013a). Most of these works study sample of galaxies selected on the basis of their elliptical morphology.

In fact, the reason for these different results is not easily detectable. A major point to be considered is that a selection based on the passivity (or on Sersic index $n > 2.5$, see, e.g., Buitrago et al. 2013) includes in the sample a significant fraction ($> 30\%$) of disk galaxies (e.g. van der Wel et al. 2011; Ilbert et al. 2010; Cassata et al. 2011; Tamburri et al. 2014) and, concurrently, does not include all the galaxies visually classi-

* adriana@lambrate.inaf.it

fied as ellipticals. At the same time, a selection based on a cut in sSFR constant with time (usually $\text{sSFR} < 10^{-11} \text{ yr}^{-1}$) selects predominantly red spheroids at $z \sim 2$ but includes a large contamination of disk/spiral galaxies in the local universe (Szomoru et al. 2011). Actually, Keating et al. (2015) show that the properties of high- z ETGs are highly sensitive to the definitions used in selecting the samples (see also Moresco et al. 2013).

On top of this debated issue on the amount of evolution in size, its possible origin is also investigated. Is the increase of the mean size due to the size-growth of individual galaxies across the time (resulting from an inside-out stellar matter accretion due to minor dry merging) or rather to the addition of new and larger galaxies over the cosmic time (e.g. Valentinuzzi et al. 2010; Carollo et al. 2013)? A promising approach to shed light on the origin of the size evolution is to investigate how the number density of dense galaxies evolves over the cosmic time (Saracco et al. 2010; Bezanson et al. 2012; Cassata et al. 2013; Poggianti et al. 2013b; Carollo et al. 2013; Damjanov et al. 2014, 2015). The analysis by different authors slightly differ in the selection of the sample (e.g. passivity, visual classification, colour, Sersic index) in the definition of “dense” galaxies (e.g. selected on the basis of their mean stellar mass density $\Sigma = M_\star/2\pi R_e^2$ or of the sigma deviation from the local size-mass relation (SMR)), and in the treatment of the progenitor bias. Saracco et al. (2010) find that the number density of dense (1σ below the local SMR) massive ($M_\star > 3 \times 10^{10} M_\odot$) ellipticals (visually selected) at $0.9 < z < 1.9$ is comparable with that of equally dense ones in local clusters. In the same direction, Poggianti et al. (2013b) studying the number density of massive ($M_\star \geq 10^{10} M_\odot$) compact ($\text{Log}(M_\star/R_e^{-1.5}) \geq 10.3 M_\odot \text{kpc}^{-1.5}$) local old galaxies find that it is just a factor 2 lower than that of compact passive galaxies observed at $z = 2$. On the opposite side, van der Wel et al. (2014) find that the number density of dense ($R_e/(M_\star/10^{11} M_\odot) < 1.5 \text{ kpc}$) massive ($M_\star > 5 \times 10^{10} M_\odot$) passive galaxies decreases by a factor ~ 10 from $z \sim 2$ at $z \sim 0.2$.

Actually, the individual size growth is expected to be more efficient for the most massive ($M_\star > 10^{11}$) galaxies. In fact, these systems are expected to host the center of the most massive halo, and to evolve mainly through minor mergers (Hopkins et al. 2009). However, given the fact that at each redshift the most massive galaxies are extremely rare (see, e.g., Muzzin et al. 2013), very few works have investigated the number density evolution of their dense subpopulation over the cosmic time. Carollo et al. (2013) find that the number density of passive ($\text{sSFR} < 10^{-11} \text{ yr}^{-1}$) and elliptical galaxies with $M_\star > 10^{11} M_\odot$ and $R_e < 2 \text{ kpc}$ decreases of $\sim 30\%$ in the 5 Gyr between $0.2 < z < 1$. An even mild evolution is claimed by Damjanov et al. (2015), who find for the passive (colour selected), dense ($\text{Log}(M_\star/R_e^{-1.5}) \geq 10.3 M_\odot \text{kpc}^{-1.5}$) galaxies with $M_\star > 8 \times 10^{10} M_\odot$ an almost constant number density in the range $0.2 < z < 0.8$.

What is still missing is a study of the number density of the “pure” elliptical (elliptical and spheroidal galaxies, visually selected, hereafter ETGs) massive ($M_\star > 10^{11} M_\odot$) dense population over the time, and in particular at $z > 0.8-1$, the range in which most of the evolution of spheroidal galaxies occurs.

In this paper, we want to probe the mass accretion history of these most massive and dense ($M_\star > 10^{11} M_\odot$, $\Sigma > 2500 M_\odot \text{pc}^{-2}$) ETGs over the last ~ 9 Gyr, by tracing the evolution of their comoving number density and by comparing their structural and dynamical parameters from redshift 1.6 to ~ 0 . One of the aspects of this work which differs from the previous analysis is the selection of the samples based on the visual classification (or on methodology which can mimic the visual clas-

sification) over the whole redshift range. In fact, the star formation histories of the galaxies are often more complex than we model them, being characterized by bursty star formation histories against smooth and gentle declining ones. As a consequence of this, in a phase of low star formation activity, an active galaxy can just “temporarily” show red colours and/or low sSFR. Moreover, galaxies tend to become passive with time. Hence, the population of passive galaxies collects a different mix of morphological types at different redshift. This leads to a non homogeneous comparison of their properties at different time (see, e.g., Huertas-Company et al. 2013). In this context, the spheroidal shape of a galaxy is a more stable property over the time and allows us to select the same population over the cosmic time. In addition, we have selected dense galaxies on the basis of their Σ rather than using a constant cut in R_e or on the basis of their deviation with respect to the local SMR. The main reason for this choice is that the mean stellar mass density, up to $z \sim 1.5$, is better correlated to, e.g., the age, the sSFR of the galaxy (Franx et al. 2008; Wake et al. 2012) and hence constitutes a more meaningful parameter.

We have organized the analysis in two parts.

The first one (see Sec. 2), is focused on the evolution of the number density of ultramassive dense ETGs over the redshift range $0 < z < 1.6$ to investigate whether the ultramassive dense high- z ETGs are numerically consistent with those observed at $z \sim 0$, or on the contrary they numerically decrease along the time suggesting an individual growth of the galaxies. For this purpose, we have referred to SDSS DR4 survey to constrain the number density of ultramassive dense ETGs at $z \sim 0.1$ paying particular attention to the bias affecting the catalog (see Sec. 2.3), and to COSMOS field to cover the range $0.2 \lesssim z \lesssim 1$ (see Sec. 2.2). For the highest redshift bin ($1.2 \lesssim z < 1.6$) we have considered two different surveys of similar area ($\sim 150 \text{ arcmin}^2$), the GOODS-South (Giavalisco et al. 2004) and the MUNICS (Drory et al. 2001), in order to average over the cosmic variance (see Sec. 2.1).

The second part of the paper is focused on the comparison of the structural (i.e. R_e , M_\star) and dynamical (i.e. velocity dispersion σ) parameters of ETGs over the last 9 Gyr (see Sec. 3). The aim of this analysis is to assess whether high- z ultramassive dense ETGs have counterparts at lower z characterized by the same structural and dynamical properties or rather some of them are not present at later epochs. To perform this comparison we have selected data from literature (see Sec. 3.1). Clearly, the request of available velocity dispersion drastically reduces the statistic of the sample at $1.2 < z < 1.6$ to 11 ETGs. For 4 of them (plus one at $z = 1.9$) we present here the new measurements of velocity dispersions (see Sec. 3.1). In Sec. 4 we summarize the work and present our results and conclusions.

Throughout the paper we adopt standard cosmology with $H_0 = 70 \text{ km s}^{-1} \text{ Mpc}^{-1}$, $\Omega_m = 0.3$ and $\Omega_\Lambda = 0.7$, the stellar mass we report are derived using the Chabrier Initial Mass Function (IMF) (Chabrier 2003) and magnitude are in the AB system when not otherwise specified.

2. The number density of ultramassive dense ETGs

In this section we constrain the stellar mass accretion history of ultramassive ETGs investigating the evolution of their number density ρ over the last ~ 9 Gyr. Since we cover the redshift range from 1.6 to 0 using different surveys (with, e.g., different magnitude cut and completeness) in Tab. 1 we summarize their main characteristics, and the references for the main quantities involved in this part of analysis (i.e., stellar mass, and R_e). As

Table 1. The main characteristics of the surveys used to derived the number density evolution from $z = 1.6$ to $z \sim 0$. *Column 1:* Name of the survey, *Column 2:* Selection criteria, *Column 3:* redshift range probed by the survey in our analysis, *Column 4:* Level of completeness for galaxies with $M_\star > 10^{11}M_\odot$ in the redshift range probed, *Column 5 (6):* Reference adopted for stellar mass (R_e) estimates, *Column 7:* Filter of the images used to derived the R_e . In all the surveys, stellar masses have been derived through the fit of the spectral energy distribution, and effective radius fitting a Sersic profile to the images.

Name	Selection criteria	redshift range probed	$M_\star > 10^{11}M_\odot$ completeness	M_\star reference	R_e reference	R_e filter
MUNICS	$K < 20.4$ & $R - K \lesssim 3.6^*$	$1.2 \lesssim z < 1.6$	100%	Sec. 3.1	Longhetti et al. (2007)	F160W/HST
GOODS-South	$K_s < 22.5$	$0.65 < z < 1.6$	100%	Tamburri et al. (2014)	Tamburri et al. (2014)	F850LP/HST
COSMOS	$F814W < 22.5$	$0.2 < z < 1.0$	100% up to $z \sim 0.8$ $\sim 80\%$ at $0.8 < z < 1.0$	Ilbert et al. (2013)	Sargent et al. (2007)	F814W/HST
SDSS	$r < 16.8$	$0.063 < z < 0.1$	100%	MPA - JHU**	Blanton et al. (2005)	r

* the color cut remove from the sample the less dense systems, so does not compromise the selection of dense ETGs. **<http://www.mpa-garching.mpg.de/SDSS/DR7/>

a reminder, we highlight that the analysis presented in this paper is aimed to probe the evolution of “ETGs”, i.e. elliptical and spheroidal galaxies selected on the basis of the visual classification. When this classification is not feasible, we have explicitly discussed it in the text.

2.1. The number density of ultramassive dense ETGs at $1 \lesssim z < 1.6$

For the comoving number density of ultramassive dense ETGs at $z > 1$, we have referred to two samples of ETGs, one selected in the MUNICS-S2F1 field, and published in Saracco et al. (2005) and Longhetti et al. (2007), and the other selected in the GOODS South-field and described in Tamburri et al. (2014).

MUNICS sample - The MUNICS sample consists of 7 ultramassive dense ETGs spectroscopically confirmed at $z \sim 1.5$. These galaxies were observed as part of the spectroscopic follow up of the complete sample of 19 extremely red objects (EROs, $K \lesssim 20.4$, $R-K \lesssim 3.6$) in the S2F1 field (Saracco et al. 2005). We have checked whether the cut both in magnitude and colour of the MUNICS sample affect our selection of ultramassive dense ETGs. Using the sample of ETGs in the GOODS-South field presented in Tamburri et al. (2014) (see below), we have verified that a sample of ETGs brighter than $K = 20.4$ is 100% complete up to $z \sim 1.6$. For what concerns the colour cut, it tends to deprive the massive sample of the less dense systems (to which we are not interested in), since the redder the colour of a galaxies, the higher its Σ (Franx et al. 2008; Saracco et al. 2011). All the galaxies of the MUNICS sample, indeed, have $\Sigma > 2500M_\odot pc^{-2}$. The effective radii of the galaxies were derived in the F160W filter with GALFIT (Longhetti et al. 2007) and the stellar masses were estimated fitting their spectral energy distribution (SED) with the Bruzual and Charlot models using the Chabrier IMF, while visual classification was performed on HST/NIC2 - F160W images (for more details see Sec. 3). We have revised the number density estimated by Saracco et al. (2005) considering only the 6 ETGs at $1.2 < z < 1.6$ in the field S2F1 (~ 160 arcmin²), thus, excluding the ETG S2F1-443 at $z = 1.91$ (see Sec. 3). We have found a comoving number density of ultramassive dense ETGs of $3.8(\pm 1.7) \times 10^{-5}$ gal/Mpc⁻³ at $1.2 < z < 1.6$, which becomes $5.6(\pm 1.9) \times 10^{-5}$ gal/Mpc⁻³ considering the spectroscopic incompleteness (a factor ~ 1.4). The errors on number densities, throughout the paper, are based on Poisson statistic.

GOODS - South sample - Given the small area of the S2F1-MUNICS field, for comparison, and to average the cosmic variance, we have also derived the number density of ultramassive dense ETGs in the GOODS-South field covering an area (143 arcmin²) comparable to the S2F1 field. To this end, we have used the sample of galaxies visually classified as ETGs on ACS/F850LP images and studied by Tamburri et al. (2014). The sample contains all the ETGs in the GOODS-South field brighter than $K_s = 22$ and for masses $M_\star > 10^{11}M_\odot$ is 100% complete up to $z \sim 2$ (Tamburri et al. 2014). Their stellar masses were derived assuming Bruzual and Charlot models and both the Salpeter IMF and the Chabrier IMF. We refer to the latter in our analysis. We have found a number density of ultramassive dense ETGs of $1.8(\pm 1.3) \times 10^{-5}$ gal/Mpc³ in the redshift range $1.3 \lesssim z < 1.6$ and of $2.9(\pm 1.6) \times 10^{-5}$ gal/Mpc³ in the redshift range $0.95 < z < 1.25$. It is worth noting that the structural parameters in the Tamburri’s et al. sample have been derived on the ACS-F850LP images with GALFIT. Hence the selection of ETGs could be biased against dense ETGs due to their larger apparent size ($\sim 30\%$, Gargiulo et al. 2012) at this wavelength. However, even correcting the effective radius of massive ETGs in the GOODS sample for this difference, the number density of dense ETGs does not change. In Table 1 and in Fig. 2 we report the measures.

2.2. The number density of ultramassive dense ETGs at intermediate redshift

In order to derive the comoving number density of ultramassive dense ETGs at intermediate redshift, we took advantage of the COSMOS survey. We have considered the catalogue of Davies et al. (2015) including all the available spectroscopic redshifts in the COSMOS area, the catalogue of structural parameters based on the HST-ACS images in the F814W filter of Scarlata et al. (2007) and the catalogue including the stellar masses of Ilbert et al. (2013) based on the multiwavelength UltraVISTA photometry. The cross match of these three catalogues produced a sample of 110171 galaxies in the magnitude range $19 < F814W < 24.8$ over the 1.6 deg² of the HST-ACS COSMOS field. We have then selected all the galaxies (25262) brighter than $F814W < 22.5$ mag for which structural parameters and morphological classification are robust (Sargent et al. 2007; Scarlata et al. 2007). From this sample we have finally extracted our parent sample of 1412 galaxies with stellar mass $M_\star > 10^{11}M_\odot$ and early-type morphology. For the morphological classi-

Table 2. The number density ρ of ultramassive dense ($M_\star > 10^{11} M_\odot$, $\Sigma > 2500 M_\odot \text{pc}^{-2}$) ETGs from $z = 1.6$ to ~ 0 . *Column 1:* redshift range; *Column 2:* number of massive dense ETGs; *Column 3:* number density of ultramassive dense ETGs; *Column 4:* error on the number density quoted; *Column 5:* field. The number density derived both in the SDSS and in the MUNICS field is a lower limits.

z	N	ρ 10^{-5} Mpc^{-3}	σ_ρ 10^{-5} Mpc^{-3}	Field
0.066 - 0.1	124	0.75	0.07	SDSS
0.2 - 0.4	13	2.6	0.9	COSMOS
0.4 - 0.6	14	1.9	0.5	COSMOS
0.6 - 0.8	39	3.6	0.7	COSMOS
0.8 - 1.0	79	4.7	0.8	COSMOS
0.95 - 1.25	3	2.9	1.6	GOODS-South
1.3 - 1.6	2	1.8	1.3	GOODS-South
1.26 - 1.6	6	3.81	1.7	MUNICS

fication we refer to the ZEST (Zurich Estimator of Structural Types) estimates by [Scarlata et al. \(2007\)](#). ZEST is an automated tool for the galaxies classification which uses the Principal Component Analysis to store the full information provided by the entire set of five basic non-parametric diagnostics of galaxy structure (symmetry, concentration, Gini coefficient, 2nd-order moment of the brightest 20% of galaxy pixels, and the ellipticity) plus the Sersic index. The software subdivided the galaxies in three main classes: early-types (type = 1), disk galaxies (type = 2) and irregular galaxies (type = 3). The robustness of the software was tested both on ~ 56000 COSMOS galaxies and on local galaxies visually classified, with excellent results. For our analysis, thus, we have selected as COSMOS ETGs all the galaxies with ZEST-type = 1. Among these, 551 have a secure spectroscopic redshift (parameter $Z_USE \leq 2$ in [Davies et al. 2014](#) catalogue), and 145 at $0.2 < z < 1.0$, have $\Sigma \geq 2500 M_\odot \text{pc}^{-2}$. As further check on morphology, we have visually classified on the HST/F814W-ACS images ([Koekemoer et al. 2007](#)) the 145 ultramassive dense COSMOS galaxies with ZEST-type = 1. Actually, we have found that all but one are ETGs.

The selection at $F814W < 22.5$ mag implies that for masses $M_\star > 10^{11} M_\odot$ the sample is 100% complete up to $z \sim 0.8$ (80% complete to $z \sim 1$). The stellar masses of [Ilbert et al. \(2013\)](#) are based on the Bruzual and Charlot (2003) models and the Chabrier IMF, consistently with our assumptions. The structural parameters of [Sargent et al. \(2007\)](#) are based on a Sersic profile fitting as in our analysis even if performed with GIM2D instead of GALFIT. However, [Damjanov et al. \(2015\)](#) show that the two methods, GIM2D and GALFIT, are in excellent agreement when based on a single Sersic component, as in our case. In order to derive the number densities of massive ETGs, we have applied a correction for the spectroscopic incompleteness that we have defined as the ratio between the magnitude distribution (in bin of 0.1 mag) of the parent sample of elliptical galaxies and the sample of ellipticals with spectroscopic redshift. In table 2 we report the comoving number density of ultramassive dense ETGs from $z = 0.2$ to $z = 1.0$, estimated in bin of redshift of 0.2 (see also Fig. 2). It is worth noting that at $z > 0.6$ the rest-frame wavelength sampled by the F814W filter is significantly different from the one sampled by the filter F160W at $z = 1.5$. However, as done for the GOODS-south data, we verified that the number densities derived from the COSMOS data at $z > 0.6$ do not change even assuming a correction of 30% of the effective radius of galaxies.

2.3. The number density of ultramassive dense ETGs in local universe

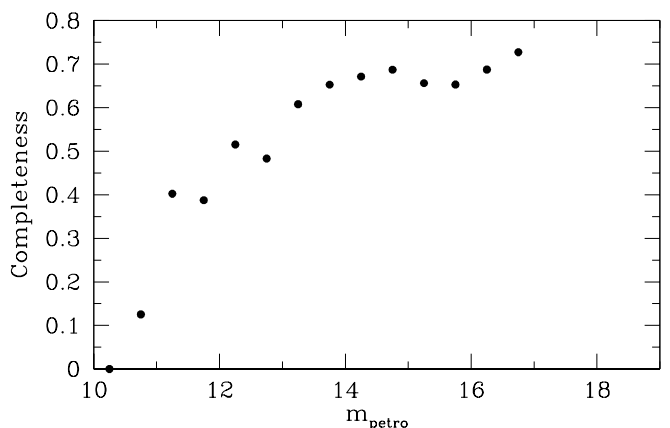


Fig. 1. The completeness of the spectroscopic SDSS galaxy catalogue with respect to the Main Galaxy Sample as a function of galaxy Petrosian magnitude.

As representative sample of local ETGs we have chosen the dataset analyzed by [Thomas et al. \(2010\)](#)¹. The authors have collected a sample of 16502 ETGs extracted from the magnitude limited sample ($r < 16.8$) of 48023 galaxies selected from the SDSS Data Release 4 ([Adelman-McCarthy et al. 2006](#)) in the redshift range $0.05 \leq z \leq 0.1$. Contrary to the other available samples, this sample is the only one in which ETGs are selected through a visual inspection of SDSS multiband images as we did for high- z ETGs. The sample is 100% complete at $M_\star > 10^{11} M_\odot$. We have associated to each ETG its stellar mass taken from MPA-JHU catalogue² and obtained through the fit of the multiband photometry (Chabrier IMF), as for the higher redshift galaxies. For the effective radius we have adopted as reference the NYU-VAG catalogue ([Blanton et al. 2005](#)). In appendix A we discuss about the robustness and limits of these estimates.

We bear in mind that the galaxy spectroscopic SDSS survey is biased against dense galaxies (e.g. [Strauss et al. 2002](#); [Poggianti et al. 2013a](#); [Taylor et al. 2010b](#)). Briefly, the “main galaxy sample” (MGS) of galaxy target for the spectroscopic follow up is composed by all the galaxies detected at $> 5\sigma$ in the r band with Petrosian magnitude $m_{\text{pet},r} < 17.77$ and r -band Petrosian half-light surface brightness $> 24.5 \text{ mag arcsec}^{-2}$. On these first cuts, three further selection criteria have been imposed to reject stars, to avoid the cross talk and to exclude bright objects that can saturate the CCD. [Taylor et al. \(2010b\)](#) have investigated how these cuts affect the distribution of local galaxies in the size mass plane and have shown that at $z < 0.05$, galaxies with masses and sizes similar to those of $z \sim 2$ galaxies are not targeted for the spectroscopic follow-up. Nonetheless, this incompleteness decreases at increasing redshift: at $z \geq 0.06$, on average, the completeness of the spectroscopic survey for compact massive galaxies is $\sim 80\%$. For this reason, we have selected from the Thomas et al.’s catalogue, all the ultramassive dense ETGs at $0.063 < z < 0.1$ (156 galaxies). Based on the evidence of Fig. A.2 we have removed from this sample those classified as ultramassive outliers in Appendix A (22 galaxies), i.e. galaxies that should not be included in the local ultramassive

¹ <http://www.icg.port.ac.uk/~thomasd/theses.html>

² <http://www.mpa-garching.mpg.de/SDSS/DR7/>

sample since, most probably, their stellar masses derived through the SED fitting are overestimated. We have visually checked this final subsample of 124 galaxies (156 - 22), and have found that no galaxy has a close companion, or is in the halo of a bright star, or is involved in a merger, factors that can alter the estimate of the effective radius. However, we have noted that $\sim 15\%$ of the sample (20 galaxies) has a not clear elliptical or S0 morphology, despite they are included in the Thomas et al.'s ETGs sample. We have checked the structural parameters of these galaxies, and they have a mean Sersic index $n \approx 3.5$ (for all the galaxies $n > 2.5$) consistent with the light profile of a spheroidal galaxy, but an axis ratio $b/a < 0.4$. Since the Blanton's catalogue does not provide the axis ratio, we have used the one obtained from the SDSS pipeline, fitting the real galaxies with a de Vaucouleur profile. Actually, the b/a should be not dependent of the surface brightness law used to fit the profile. We have left these elongated objects in the final sample, since the Thomas et al. sample is widely adopted, and studied, but in Sec. 2.4 we show that this choice does not impact our results.

Beside this source of incompleteness due to the targets selection, we have to consider that not all the spectroscopic target were actually observed (for example because two fibres cannot be placed closer than $55''$ on a given plate). This source of incompleteness should be more important for the brightest galaxies and should be taken into account in the derivation of the comoving number density. To quantify it we have extracted the MGS from DR4 database restricting the query to only the sciencePrimary objects (in order to reject the multiple observations, 648852 galaxies). From this sample we have rejected galaxies classified as quasar remaining with 636980 galaxies. Among these objects 384564 ($\sim 60\%$) have been spectroscopically observed and $\sim 88\%$ of them has secure redshift (i.e. $z_{\text{warning}} = 0$). We have defined the completeness in bin of magnitude as the ratio of galaxies with secure redshift, over the number of galaxies in the MGS (see Fig. 1). Taking in consideration this, we have found a number density for local ultramassive dense ETGs of $0.75(\pm 0.07) \times 10^{-5} \text{ gal/Mpc}^{-3}$. We have repeated the measure of ρ assuming as stellar masses for local ETGs those derived by Kauffmann et al. (2003) with spectral indices - see Appendix A - and we have found $\rho = 0.7(\pm 0.06) \times 10^{-5} \text{ gal/Mpc}^{-3}$. We have corrected the number density for the incompleteness of the spectroscopic sample with respect to the MGS but we remind that the original selection cuts of the MGS can exclude part of massive dense ETGs especially in the lowest redshift bin. The number density we quote is therefore a lower limit.

2.4. The evolution of the number density of ultramassive dense ETGs over the last 9 Gyr: results

Figure 2 shows the evolution of number density for the ultramassive dense ETGs in the last ~ 9 Gyr. Once the possible sources of non-homogeneity are taken into account the mean value of the number density of ultramassive dense ETGs, within the uncertainties, is $\sim 3.0 \pm 1.5 \times 10^{-5} \text{ Mpc}^{-3}$. We observe that at $z \sim 0.8$, in the COSMOS field, there is a significant overdensity (see e.g. Damjanov et al. 2015, and reference therein) and that, correspondingly, this is the point that most deviates in Fig. 2. We have fitted the number densities estimated in the redshift range $0.06 \leq z < 1.6$ with a power law, treating the SDSS and MUNICS point as lower limits, and have found $\rho(z) \propto (1+z)^{0.3 \pm 0.8}$, showing that the number density of ultramassive dense ETGs may decrease from $z=1.6$ to $z=0$, approximately by a factor 1.3. We have repeated the fit excluding from local sample those galaxies

with ambiguous morphology (see Sec. 2.3), but the slope does not change, since in the fit this point is considered a lower limit.

2.5. Comparison with previous works

The number density estimates of dense ETGs are clearly dependent on many factors, such as the stellar mass limit, the definition of compact galaxies, and the criteria adopted to select the sample (e.g. visual classification, colour, passivity). This implies that any comparison of our results with those by other authors is not straightforward. In the following we try to compare our estimates of number density with those by other authors which adopted selection criteria as similar as possible to ours. Given the many factors concurring in the final estimate of ρ , to better visualize these comparisons, in Fig. 2 we report, in the size mass plane, the stellar mass and effective radius limits of each sample. At the same time, we add a table that can immediately show the characteristics of all the samples studied.

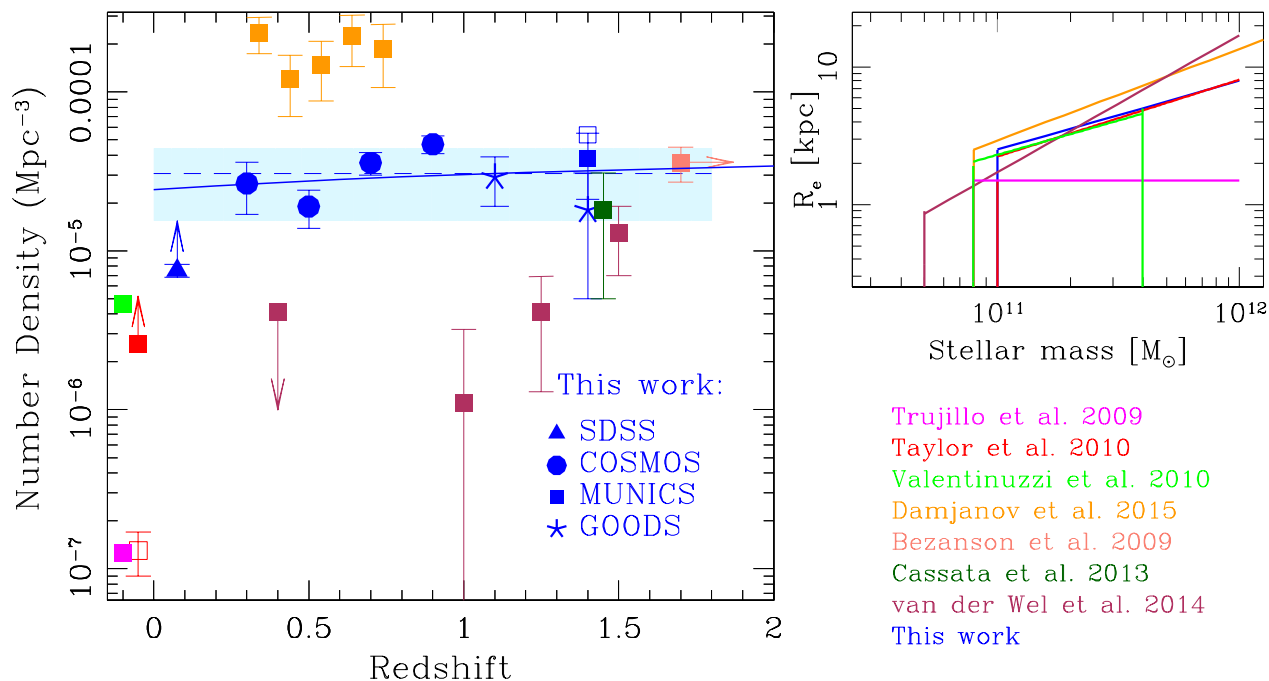
2.5.1. Local universe

For what concerns the local universe, there is a clear tension among the results already published, since the number densities derived from the SDSS database (Trujillo et al. 2009; Taylor et al. 2010a) turn out to be at least 1-2 order of magnitude lower than that derived from other database (e.g. WINGS/PM2GC) (Valentinuzzi et al. 2010; Poggianti et al. 2013b, see Fig. 2). Interestingly, Fig. 2 shows that our estimate of local number density, although derived on SDSS database, is much more in agreement with the finding of Valentinuzzi et al. (2010) than with that by Trujillo et al. (2009) and Taylor et al. (2010a). In the following, we investigate the possible origins of the observed discrepancy.

In fact, Taylor et al. (2010a) search for counterparts of high- z compact massive galaxies in the DR7 SDSS spectroscopic database. To this aim, they select from the sample of local galaxies at $0.066 < z < 0.12$, with $M_{\star} > 10^{10.7} M_{\odot}$, and $\log(R_{e,z}/\text{kpc}) < 0.56 \times (\log(M_{\star}/M_{\odot}) - 9.84) - 0.3$ (i.e. with radius in the SDSS- z band at least twice smaller than the local SMR by Shen et al. (2003)), those with $^{0.1}(u-r) > 2.5^3$, in order to select the descendant candidates of high- z dense galaxies. They reject from their sample all the galaxies with possible problems with their size measurement (due to confusion with, e.g., other galaxies, or with extended halos and/or with spikes of bright stars) or mass estimate, for a total final sample of 63 galaxies. Among these galaxies, 11 have stellar mass $> 10^{11} M_{\odot}$ and yield a number density of $1.3(\pm 0.4) 10^{-7} \text{ gal/Mpc}^3$ over the entire volume of the SDSS-DR7 spectroscopic survey (see FIG. 2 open red square). This value, not corrected for the spectroscopic incompleteness of SDSS-DR7 survey, is \sim two orders of magnitude lower than the one we have found. Actually, this huge observed difference cannot be ascribed only to the completeness function. In fact, it is really difficult to pinpoint the origin of such a difference between our and their result, since the two samples are differently selected.

In fact, the cut they apply in R_e is very similar to our cut in Σ (see size mass plane in Fig. 2), however, differently from us they select only red galaxies. To test the impact of the colour selection, we have computed the $^{0.1}(u-r)$ colour for the galaxies of our sample and have found that all but one have $^{0.1}(u-r) > 2.5$, so the colour selection cannot be the source of the observed

³ the superscript 0.1 indicates rest-frame photometry redshifted to $z = 0.1$, (see, e.g., Blanton & Roweis 2007)



Reference	z	Stellar mass range	Compactness definition	Supplementary galaxy selections
This work	$0 \lesssim z \lesssim 1.6$	$M_* > 10^{11}$	$\Sigma \geq 2500 \text{ M}_\odot \text{pc}^{-2}$	Elliptical morphology (Visual classification)
Trujillo et al. (2009)	$0 < z < 0.2$	$M_* > 8 \times 10^{10}$	$R_e < 1.5 \text{ kpc}$	–
Taylor et al. (2010)	$0.066 < z < 0.12$	$M_* > 10^{11}$	$\log(R_{e,z}/\text{kpc}) < 0.56 \times (\log(M_*/M_\odot) - 9.84) - 0.3$	$(u - r) > 2.5$
Valentinuzzi et al. (2010)	$0.04 < z < 0.07$	$8 \times 10^{10} < M_* < 4 \times 10^{11} \text{ M}_\odot$	$\Sigma > 3000 \text{ M}_\odot \text{pc}^{-2}$	–
Damjanov et al. (2015)	$0.2 < z < 0.8$	$M_* > 8 \times 10^{10}$	$\log(R_e/\text{kpc}) < 0.568 \times \log(M_*/M_\odot) - 5.74$	NUVrJ colours
Bezanson et al. (2009)	$z = 2.5$	$M_* > 10^{11}$	–	Quiescent
Cassata et al. (2013)	$1.2 < z < 1.6$	$M_* > 10^{11}$	$\Sigma \geq 2500 \text{ M}_\odot \text{pc}^{-2}$	sSFR $< 10^{-11} \text{ yr}^{-1}$ + elliptical morphology
van der Wel et al. (2014)	$0 \lesssim z \lesssim 1.6$	$M_* > 5 \times 10^{10}$	$R_e/(M_*/10^{11} \text{ M}_\odot)^{0.75} < 1.5 \text{ kpc}$	UVJ red colours

Fig. 2. *Top - left:* The evolution of the comoving number density of ultramassive dense ETGs ($M_* > 10^{11} \text{ M}_\odot$, $\Sigma > 2500 \text{ M}_\odot \text{pc}^{-2}$) from redshift 1.6 to redshift ~ 0 (blue symbols). The open blue square indicates the number density of ultramassive dense MUNICS ETGs at $z > 1.4$ corrected for the spectroscopic incompleteness of the MUNICS survey (see text). Solid blue line is the best fit relation to our data in the range $0.066 < z < 1.6$ ($\rho \propto (1+z)^{0.3}$), while blue dotted line indicates the mean value over the redshift range $0.066 < z < 1.6$ (dashed area marks the 1σ deviation around this value). Orange squares are the number density for ultramassive compact galaxies by Damjanov et al. (2015), magenta one by Trujillo et al. (2009), light green one by Valentinuzzi et al. (2010), purple ones by van der Wel et al. (2014), salmon one by Bezanson et al. (2009), dark green one by Cassata et al. (2013), and open red square by Taylor et al. (2010a). The points by Taylor et al. (open red square) and Cassata et al. (dark green square) are derived selecting from their sample only the galaxies with $M_* > 10^{11} \text{ M}_\odot$ (see Tab. in the figure). Filled red square is the number density by Taylor et al. obtained using the circularized Sersic R_e . *Top - right:* The cuts in R_e and M_* of our and others samples in the size mass plane (colours are the same in the top - left panel). *Bottom table:* A quick comparison of the main characteristics of our sample with respect to those by other authors we compare. *Column 1:* reference paper, *Column 2:* redshift range, *Column 3:* stellar mass limits (for Taylor et al. and Cassata et al. is reported the one we use), *Column 4:* compactness definition, *Column 5:* other supplementary selections applied to the samples.

difference in the number density. We have then investigated the impact on the number density of the different R_e used. Actually, we use the *circularized* R_e obtained fitting the surface brightness profile with a Sersic law (hereafter $R_{e,Ser}$), instead of the semi-major axis SM_e , used by Taylor et al., obtained from SDSS

pipeline fitting the SDSS images with a de Vaucouleur profile (hereafter $SM_{e,dV}$). For this reason, we have repeated their analysis looking for differences in the ρ estimates varying the definition of R_e . To do this, we have selected from the primary observations of the DR7 spectroscopic sample the 226312 galax-

ies with secure redshift (i.e. $z_{\text{warning}} = 0$) and spectroscopic redshift $0.066 < z_{\text{spec}} < 0.12$. Among them, we have collected those with $M_{\star} > 10^{11}M_{\odot}$, $\log(SM_{e,dV}/\text{kpc}) < 0.56 \times (\log(M_{\star}/M_{\odot}) - 9.84) - 0.3$, and $^{0.1}(u-r) > 2.5$. For the $SM_{e,dV}$, consistent with Taylor et al., we retrieve the catalogue from the SDSS database, while for the stellar masses derived through the SED fitting, we refer to the MPA - JHU catalogue (see Sec. 2.3). We have visually inspected this subsample, and we have rejected all the galaxies with problems related with the size measurement (e.g. merging galaxies, or close pairs or galaxies in the halo of a bright stars), leaving us with 49 galaxies. None of them is a quasar. To check the reliability of the stellar mass estimates we have applied the same procedure of Appendix A. Among the 49 galaxies of our selection, 38 have a stellar mass estimate derived also from the spectral indices (stellar masses from spectral indices were derived only for galaxies in the DR4 database), and for 10 of them ($\sim 26\%$) the two estimates are consistent. These ten galaxies are all included in the subsample of 11 massive galaxies of Taylor and collaborators. Assuming that the fraction of galaxies with consistent estimates of M_{\star} is constant, we should expect ~ 12 galaxies (49×0.26) with $M_{\star} > 10^{11}M_{\odot}$, $\log(SM_{e,dV}/\text{kpc}) < 0.56 \times (\log(M_{\star}/M_{\odot}) - 9.84) - 0.3$, $^{0.1}(u-r) > 2.5$ in DR7 release, in agreement with Taylor and collaborators. When circularized SDSS de Vaucouleur radii ($R_{e,dV}$) are instead used, we have found 569 galaxies with $M_{\star} > 10^{11}M_{\odot}$, $\log(R_{e,dV}/\text{kpc}) < 0.56 \times (\log(M_{\star}/M_{\odot}) - 9.84) - 0.3$, $^{0.1}(u-r) > 2.5$, among which 186 have good R_e estimates and stellar mass, against the 12 found when semi-major axes are used. Finally, when we use the Blanton's $R_{e,Ser}$ (circularized and obtained fitting a Sersic profile), we find 687 galaxies with $M_{\star} > 10^{11}M_{\odot}$, $\log(R_{e,Ser}/\text{kpc}) < 0.56 \times (\log(M_{\star}/M_{\odot}) - 9.84) - 0.3$, and $^{0.1}(u-r) > 2.5$, which after all the checks and the visual inspection, result in a final sample of ~ 224 galaxies, a factor > 20 higher than the one obtained using the semi-major axis. The higher number of galaxies we have found using $R_{e,Ser}$ with respect to the one obtained using circularized de Vaucouleur radius is consistent with the expectations. Compact galaxies are known to generally have Sersic index $n < 4$, thus, the value of R_e obtained fitting a de Vaucouleur profile should be higher with respect to that obtained fitting a Sersic law. This implies that the number of compact objects, defined using a ‘‘Sersic’’ - R_e should be greater than that obtained using a ‘‘de Vaucouleur’’ - R_e , as we find. For more details on the comparison of the local samples selected using circularized R_e and semi-major axis (SM_e), or de Vaucouleurs and Sersic R_e see Appendix B. Thus, these checks show that the much lower number density found by Taylor et al. with respect to our estimate is due to the fact that they use the semi-major axis. Once the circularized Sersic R_e are used, the number density (not corrected for spectroscopic incompleteness) increases up to $2.6(\pm 0.2)10^{-6}$ gal/Mpc $^{-3}$, qualitatively in agreement with our estimate.

Trujillo et al. (2009), from the analysis of the SDSS DR6 database, claim that only the 0.03% of galaxies at $z < 0.2$ with $M_{\star} > 8 \times 10^{10}M_{\odot}$ have $0.05'' < R_e < 1.5$ kpc. We have found that among the 99783 galaxies in the SDSS DR4 spectroscopic sample with $z < 0.2$, $z_{\text{warning}} = 0$ and $M_{\star} > 8 \times 10^{10}M_{\odot}$, only 113 (i.e. $\sim 0.11\%$ of the massive sample) have $0.05'' < R_e < 1.5$ kpc. The visual inspection rejects 76 galaxies since e.g. in the halo of a bright star, or a merger galaxy. This leave a sample of 37 galaxies, i.e. the 0.037% (vs 0.03% by Trujillo) of the original sample of local galaxies with $M_{\star} > 8 \times 10^{10}M_{\odot}$. In this case, thus, the difference we have found among our estimate and the one by Trujillo et al. is to totally ascribed to the different selection criteria. The authors probe a region of the size-mass plane included in our region (see size mass plane in Fig. 2) and known to be highly

incomplete in the SDSS spectroscopic survey. Both factors lead to a very low number density.

Valentinuzzi et al. (2010) studying the sample of 78 clusters included in the WINGS survey, have derived the number density of local ($0.04 < z < 0.07$) galaxies with $8 \times 10^{10} < M_{\star} < 4 \times 10^{11}M_{\odot}$ and $\Sigma > 3000M_{\odot}\text{pc}^{-2}$. Assuming no dense massive galaxies outside the clusters, they found a hard lower limit to the number density of these systems of 0.46×10^{-5} gal/Mpc $^{-3}$. Using the DR7, we have found 181 galaxies in the same $z/M_{\star}/\Sigma_g$ range, where Σ_g is the mean stellar mass density derived using the effective radius measured by Blanton on SDSS g -band images, i.e. the SDSS band that gets closer to the v -band used by Valentinuzzi et al. (2010). Among the 181 selected galaxies, 120 have reliable structural parameters, and $\sim 64\%$ of them has a robust stellar mass estimate. Taking into account the effect of the incompleteness, we have found that the number density is $\rho = 5.21 \times 10^{-5}$ gal/Mpc 3 , thus a factor 10 higher than the lower limit of Valentinuzzi et al. (2010). Our estimate places in the right direction with respect to that of Valentinuzzi, but we are not in the position to make a more quantitative comparison. We avoid to compare our results with those by other analysis (e.g. Poggianti et al. 2013b) which, although treating the evolution of the number density of compact galaxies, adopt a much lower cut in stellar mass with respect to our (e.g. $\sim 1.5 \times 10^{10}M_{\odot}$).

2.5.2. Intermediate redshift range

Carollo et al. (2013) derive the number density of $M_{\star} > 10^{11}M_{\odot}$ quenched ($s\text{SFR} < 10^{11}\text{yr}^{-1}$) and elliptical galaxies with $R_e < 2.5\text{kpc}$ over the redshift range $0.2 < z < 1$ and find that it decreases by a factor $\sim 30\%$. Their analysis is focused on a sample of galaxies, on average, denser than the one studied here, and differently from us they do not consider all the elliptical galaxies, but the subsample of passive ones. Despite this, their trend is in fair agreement with our findings. In fact, we find a decrease of ρ of $\sim 20\%$ in the redshift range $0.2 < z < 1.0$.

Damjanov et al. (2015) present the number density of quiescent (colour - colour selected) galaxies with $\text{Log}(M_{\star}/R_e^{1.5}) > 10.3M_{\odot}\text{kpc}^{-1.5}$ and $M_{\star} > 8 \times 10^{10}$ in the COSMOS field and find that it is roughly constant in the redshift range $0.2 < z < 0.8$. Their sample includes our one, thus, as expected their number density values are higher than those we find, but once again, their trend of ρ with z is in fair agreement with us. Actually, from $z = 0.8$ to $z = 0.2$ we find that ρ decreases by $\sim 10\%$.

2.5.3. High redshift

Bezanson et al. (2009), integrating the Schechter mass function given in Marchesini et al. (2009) find that the number density of the galaxies with $M_{\star} > 10^{11}M_{\odot}$ is $7.2^{+1.1}_{-1.1} \times 10^{-5}$ Mpc $^{-3}$ at $z = 2.5$. Assuming that \sim half of the galaxies with $M_{\star} > 10^{11}M_{\odot}$ are compact, they find that the number density of compact massive galaxies at $z = 2.5$ is $3.6^{+0.9}_{-0.9} \times 10^{-5}$ Mpc $^{-3}$. We note that the authors assume the Kroupa (2001) IMF, which provides stellar masses a factor ~ 1.2 higher than that obtained assuming the Chabrier IMF, so their value with respect to ours is an upper limit. Really interestingly the estimate by Bezanson et al. (2009) at $z = 2.5$ is in agreement with the mean value we find at $z < 1.6$ and with our best-fit.

Cassata et al. (2013) derive the number density of compact (i.e. 1σ below the local SMR) and ultracompact (more than 0.4 dex smaller than local counterparts of the same mass) passive ($s\text{SFR} < 10^{-11}\text{yr}^{-1}$) galaxies with elliptical morphology and

$M_{\star} > 10^{10} M_{\odot}$ in the ~ 120 arcmin² of the GOODS-South field covered by the first four CANDELS observations (Grogin et al. 2011; Koekemoer et al. 2011) and by the Early Release Science Program 2 (Windhorst et al. 2011). Using their published sample of 107 galaxies, we have selected the only two galaxies with $M_{\star} > 10^{11} M_{\odot}$ and $\Sigma > 2500 M_{\odot} \text{pc}^{-2}$ at $1.2 \leq z \leq 1.6$, which account for a number density of $1.47(\pm 1.04) 10^{-5} \text{ gal/Mpc}^3$. This value is slightly lower than the one we have found in the GOODS - South field (see Tab. 1), nonetheless we bear in mind that the authors selected passive *and* elliptical galaxies while we apply a pure visual classification. Tamburri et al. (2014), comparing the sample of passive galaxies with that of elliptical ones, visually classified, in the GOODS - South field, have shown that about $\sim 26\%$ of ETGs have $s\text{SFR} \geq 10^{-11} \text{ yr}^{-1}$, i.e. are not passive. Taking in consideration this, we have corrected the number density by a factor 1.26, obtaining $1.85(\pm 1.30) \times 10^{-5} \text{ gal/Mpc}^3$, in agreement with our estimate on the GOODS - South field. We note that the agreement between our number density estimate and that from Cassata's sample, although on the same field, is not straightforward. Actually, all the quantities involved in our estimate (e.g. stellar mass, effective radius) are derived independently by us. However, despite the different approaches and procedures, the number densities are consistent, reinforcing the robustness of the result.

In the 3D-HST survey, van der Wel et al. (2014) derive the number density of compact ($R_e/(M_{\star}/10^{11} M_{\odot})^{0.75} < 1.5 \text{ kpc}$) passive (on the basis of their UVJ colours) galaxies with $M_{\star} > 5 \times 10^{10} M_{\odot}$ in the redshift range $0 < z < 3$. In contrast with us, the authors find a decrease by a factor ≥ 10 from $z = 1.6$ to $z = 0$. We have to premise that a reliable comparison with their work is unfeasible given the much different criteria used to select the samples, so we cannot go deeper in the origin of the drop that can be due to, e.g., the different stellar mass limit ($M_{\star} > 5 \times 10^{10} M_{\odot}$ vs $M_{\star} > 10^{11} M_{\odot}$) and/or to a peculiarity of the population of red galaxies (in principle, we have no reason to suppose that the formation and evolutionary picture of ultramassive dense ETGs is similar to that of less massive and red galaxies). However, we find jarring that the values they find are a factor > 5 lower than ours, despite their more relaxed cut in stellar mass. In the following we simply try to understand the origin of this discrepancy. The criterion they adopted to select compact galaxies is very similar to our (see Fig. 2), as well as the reference restframe wavelength for the R_e (r -band for us and 5000 \AA for them). Thus, the reasons for the huge discrepancy we observe cannot reside in these features. There are two main differences between their and our approach. The first one is that they used the semi-major axes SM_e , instead of the R_e . The second one is that they did not directly measure the semi-major axis on images sampling the 5000 \AA rest-frame at the various redshift considered, but they derived it from the $SM_{e,F125W}$ (i.e. the semi-major axis measured on the F125W-band images) assuming a variation with λ ($\Delta \log SM_e / \Delta \log \lambda = -0.25$ (see their Eq. 2)). In order to investigate whether one of these aspects (or both) are responsible of the observed discrepancy, we have used our sample of ETGs selected in the GOODS-South field by Tamburri et al. (2014) and have derived the number densities of ultramassive dense ETGs following the recipe by van der Wel et al. (2014). In details, we have associated at each galaxy of our sample the structural parameters derived by van der Wel in both the F125W and F160W filter. From them we have estimated the $R_{e,5000\text{\AA}der}$ and the $SM_{e,5000\text{\AA}der}$ following their Eq. 2. In the redshift range $0.95 < z < 1.25$ in the GOODS South field we have found 3 galaxies with $M_{\star} \geq 10^{11} M_{\odot}$ and $\Sigma \geq 2500 M_{\odot} \text{pc}^{-2}$ (see Table 2),

while using $R_{e,5000\text{\AA}der}$ and $SM_{e,5000\text{\AA}der}$, there are no ETGs. At $1.3 < z < 1.6$ we find 2 galaxies. We have found the same number of objects using $R_{e,5000\text{\AA}der}$ and just 1 using the semi-major axis $SM_{e,5000\text{\AA}der}$. Thus, applying the same procedure by van der Wel et al. to derive the number density of ultramassive dense ETGs we find values of ρ lower or comparable (and no more higher) than the ones presented in their paper, thus much more consistent with the expectations considering the fact that our cut in stellar mass is more restrictive (for a more exhaustive analysis on the effect of the extrapolation of the SM_e using the van der Wel et al.'s Eq. 2, see Appendix C.). However, we should take in mind that in this comparison both the cosmic variance, and also the different selection of the sample (elliptical vs. passive) have a strong effect on the number density estimates. All these checks highlight the huge impact of the criteria and quantities used in the analysis on the comparison of the results. A fair comparison is really hard to address, and this stresses the impelling necessity of analysis on homogeneous samples over the cosmic time to draw firm conclusions.

3. The evolution of structural and dynamical parameters of ultramassive dense ETGs

The mild evolution in the number density shows that in local universe, the ultramassive dense ETGs are at most $\sim 25\%$ less numerous than at $\langle z \rangle = 1.4$. Thus, if a significant fraction of ultramassive dense ETGs evolves in size, new ones have to appear at lower redshift to maintain their number density almost constant. However, the observed mild number density evolution opens also to the possibility that most ($\sim 75\%$) of the ultramassive dense ETGs passively evolve from $\langle z \rangle = 1.4$ to $z = 0$. In this case, local and high- z ultramassive dense ETGs should share also the same structural and dynamical properties. In the following we compare the structural (R_e and M_{\star}) and dynamical properties (σ_e) of the ultramassive dense ETGs over the last 9 Gyr. We highlight that in this second part of analysis, we investigate the same class of objects studied in Sec. 2, so ETGs visually classified with $M_{\star} > 10^{11} M_{\odot}$ and $\Sigma > 2500 M_{\odot} \text{pc}^{-2}$. However, the request of available velocity dispersion, does not allow us to use the same samples presented in Sec. 2. In Sec. 3.1 we present the samples used for this part of analysis.

3.1. The comparison samples

In order to compare the structural and dynamical properties of ultramassive dense ETGs over the last 9 Gyr, we still refer, as local reference, to the sample of 124 ETGs presented in Section 2.3. For what concerns the stellar mass and the effective radius used, we refer to Sec. 2.3. For the velocity dispersions we have referred to DR7 σ since in DR7 there have been improvements to the algorithms which photometrically calibrate the spectra, and all spectra have been re-reduced (see Thomas et al. (2013) for more tests on the reliability of DR7 σ estimates).

For the intermediate and high- z sample, we cannot refer exactly to the same samples used to estimate the number density in Sec. 2, since not all the ETGs have available velocity dispersions. In order to probe the intermediate redshift range ($0.2 \leq z \leq 0.9$), we refer to the sample of field and cluster ETGs published by Saglia et al. (2010). The authors selected the galaxies of their sample on the basis of their spectra (requesting the total absence or the presence of only weak [OII] lines), and for those with HST images they provided also the morphological classification (T type). We have selected from their sample, the galaxies

with elliptical morphology (T type ≤ -4), and with $M_\star > 10^{11} M_\odot$ and $\Sigma > 2500 M_\odot \text{pc}^{-2}$. The stellar mass provided by the authors are derived adopting the Salpeter IMF. We have converted these estimates to Chabrier IMF scaling the masses by 0.23 dex. For the majority of the galaxies, the structural parameters were derived on the F814W-band images, while for a small fraction, I-band VLT images were used. We have integrated the Saglia et al.’s sample, with that by Zahid et al. (2015), in which passive galaxies are selected on COSMOS field using a NUVrJ color-color cut. Using the coordinates of the galaxies available at the author’s website⁴, we have visually checked their morphology on HST/ACS images, founding that all but one passive galaxies are ellipticals.

For the high- z sample, we have collected all the high- z ETGs at $1.2 < z < 1.6$ with $\Sigma > 2500 M_\odot \text{pc}^{-2}$, $M_\star > 10^{11} M_\odot$, available kinematics (i.e. velocity dispersion) and effective radius derived in the F160W band (11 objects). The morphological classification has been performed on the basis of a visual inspection of the galaxies carried out on the HST images in the F160W filter. Among the 11 galaxies of the total high- z sample 7 galaxies have been taken from the literature (see below) and for the remaining four of them (plus one at $z=1.9$, hereafter “our sample of high- z ETGs”) we present the unpublished VLT-FORS2 spectra together with their velocity dispersion measurements (Section 3.2). For what concerns the 7 galaxies from literature:

- Four ETGs are taken from Bezanson et al. (2013). From the eight galaxies of their sample we have removed the galaxy U53937 being less massive than $10^{11} M_\odot$, U55531 since its image shows that is not an elliptical, and C13412 and C22260 having $\Sigma < 2500 M_\odot \text{pc}^{-2}$.
- Two ETGs are taken from Belli et al. (2014). From the 56 quiescent galaxies of their sample, we have excluded 23 passive galaxies having $z < 1.2$; of the remaining 33, 24 have been rejected having $M_\star < 10^{11} M_\odot$, three for not being ETGs (4906, 34609 and 34265) and four (1244914, 2823, 34879, 7310) to have $\Sigma < 2500 M_\odot \text{pc}^{-2}$.
- One ETG is taken from Longhetti et al. (2014). This galaxy belongs to MUNICS sample of 6 ETGs described in Sec. 2.1 and used to estimate the number density.

The sample is summarized in Table 3. We do not include the 3 ETGs out of 17 galaxies presented in Newman et al. (2010) (ID GN3, GN4^b, GN5^b) with available σ , redshift $z > 1.26$ and $M_\star > 10^{11} M_\odot$, since their effective radii were derived fitting a de Vaucouleur and not a Sersic profile.

3.2. Our sample of high- z ETGs: spectroscopic observations and velocity dispersion measurements

The remaining four (plus one at $z=1.91$) ETGs of the total high- z sample (Fig. 3, HST-NIC2/F160W images from Longhetti et al. 2007) have been selected among the 7 ultramassive dense ETGs spectroscopically identified at $z \sim 1.5$ in the field S2F1 of the MUNICS survey (Drory et al. 2001), thus belong to the MUNICS sample we have used to constrain the number density of ultramassive dense ETGs at $z \sim 1.4$ (see Sec. 2.1). Their surface brightness profiles are derived by Longhetti et al. (2007) fitting the HST-NIC2/F160W images with a 2D-psf convoluted Sersic law with the software GALFIT (Peng et al. 2002). In Table 4 we report the effective radii of the best-fitted Sersic profile for the 5 ETGs. The circularized R_e [kpc] are slightly different from those

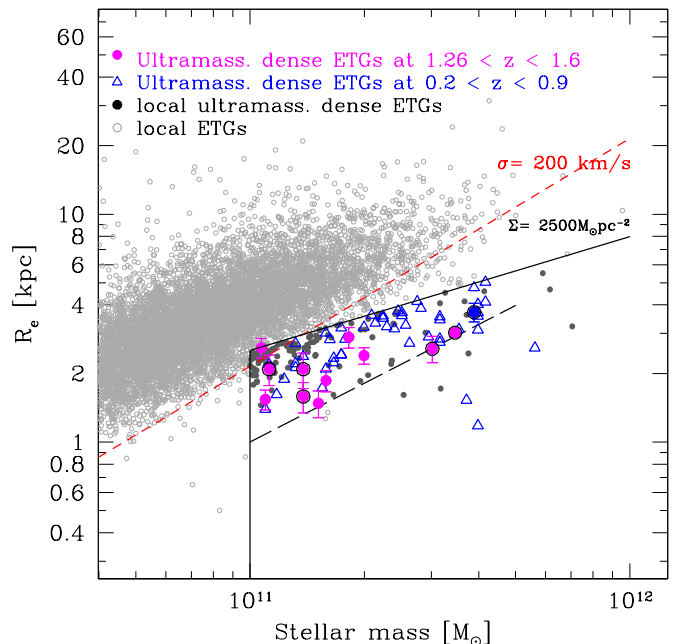


Fig. 4. The distribution of the ultramassive dense ETGs at $1.2 < z < 1.6$ (magenta filled circles), at $0.3 < z < 0.9$ (blue open squares), and in local universe (dark grey points) in the R_e - M_\star plane. Solid black lines define the cuts in M_\star and Σ of our samples. The ETGs from MUNICS sample with available velocity dispersion (5 presented here and one in Longhetti et al. (2014)) are black countered. The one at redshift 1.91 (hence not included in the analysis of Sec. 3.3) is indicated by a blue point. Small open circles are local ETGs from Thomas et al. (2010) in the redshift range $0.063 < z < 0.1$. Red line indicates a line of constant σ derived as $R_e = \sqrt{GM_\star/5\sigma}$, i.e. assuming zero dark matter. Long-dashed line indicates the lower boundary of the size-mass relation as found by Belli et al. (2014) and van der Wel et al. (2014).

published in Longhetti et al. (2007) due to the more accurate estimates of the redshift we have derived from the higher resolution VLT-FORS2 spectra. Stellar masses have been re-estimated to take into account the updated value of redshift and the now available near-IR photometry in the WISE RSR-W1 filter ($\lambda_{eff} \approx 3.4 \mu\text{m}$). We have considered a grid of composite stellar population templates derived from Bruzual & Charlot (2003) with solar metallicity Z_\odot , exponentially declining star formation history ($\propto \exp(-t/\tau)$) with star formation time scale τ in the range 0.1-0.6 Gyr and the Chabrier IMF (Chabrier 2003). The effect of dust extinction has been modelled following the Calzetti law (Calzetti et al. 2000) with A_V in the range [0.0-2.0]. The stellar masses M_\star associated to the best-fit model are reported in Table 4. For the estimates of the number density derived in Sec. 2 we have referred to these updated values of R_e and M_\star .

Spectroscopic observations of our 5 ETGs were performed with the ESO VLT-FORS2 spectrograph in MXU mode during 4 runs in 2010 and 2011. The OG590 filter and the GRIS-600z grism were adopted to cover the wavelength range $0.6 \mu\text{m} < \lambda < 1.0 \mu\text{m}$ with a sampling of 1.6 \AA per pixel. With a $1''$ slit the resulting spectral resolution is $R \approx 1400$ corresponding to a FWHM $\approx 6.5 \text{ \AA}$ at 9000 \AA . The total effective integration time on target galaxies is ~ 8 hours which results in signal-to-noise (S/N) per pixel $\sim [8-10]$ depending on the galaxy. Standard reduction

⁴ https://www.cfa.harvard.edu/~hzahid/Data_files/ApJ97868_table1.asci has been performed with IRAF tasks. In each frame the sky has

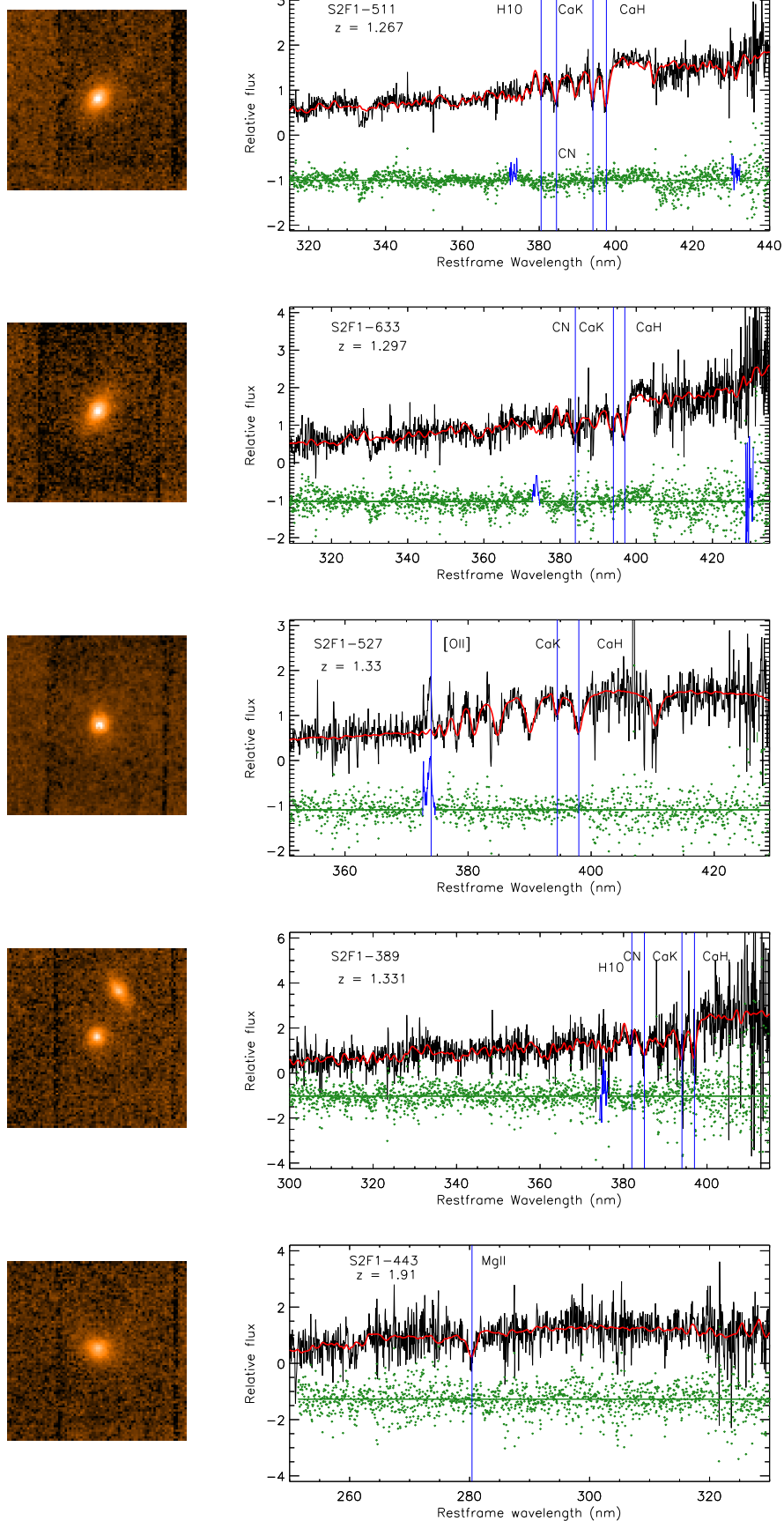


Fig. 3. *Left column:* The HST-NIC2/F160W images of the 5 ETGs of our high- z sample for which we present here the VLT-FORS2 spectra (each image is 6×6 arcsec). *Right column* Unsmoothed and not-rebinned spectra of our 5 ETGs (black lines, 8 hours of effective integration time). Many optical absorption features (blue lines) are clearly distinguishable from the continuum. The best-fit pPXF model is plotted in red. On average, pPXF selects and combines 2-4 star templates to reproduce the observed spectrum. Residuals after best-fit model subtraction are shown with green points. In the residual tracks, blue lines are the regions automatically excluded by the software pPXF as strongly affected by sky emission lines.

Table 3. Sample of high- z ETGs collected from literature. *Column1:* ID, *Column2:* RA, *Column3:* Dec, *Column4:* redshift *Column5:* circularized effective radius, *Column6:* Sersic index, *Column7:* axis ratio, *Column8:* filter adopted to derive the surface brightness parameters, *Column9:* measured velocity dispersion, *Column10:* velocity dispersion within R_e , *Column11:* Stellar masses. References for the velocity dispersion values are listed near the ID value. When a data of the galaxy comes from a paper different from the one where the σ is published, the new reference is specified near its value.

Object	RA h:m:s	Dec d:m:s	z	R_e (kpc)	n	b/a	Camera-Filter	σ (km/s)	σ_e (km/s)	$\log M_\star$ (M_\odot)
A17300 ¹	14:18:39.78	52:41:59.51	1.423	2.9 ± 0.51^2	5.3	–	HST/WFC3-F160W	265 ± 7	272 ± 7	11.26
A21129 ¹	14:19:10.56	52:46:26.79	1.583	1.5 ± 0.27^2	5.0	–	HST/WFC3-F160W	260 ± 9	278 ± 10	11.18
C21434 ¹	10:00:36.10	2:32:13.77	1.522	1.9 ± 0.33^2	3.1	–	HST/WFC3-F160W	218 ± 16	230 ± 17	11.20
C20866 ¹	9:59:18.64	2:31:39.03	1.522	2.4 ± 0.42^2	3.0	–	HST/WFC3-F160W	272 ± 23	282 ± 23	11.30
21750 ³	215.03490	52.9829	1.242	2.59 ± 0.26	5.2	0.57	HST/WFC3-F160W	–	259 ± 16	11.03
7310 ³	150.05791	2.2904	1.255	4.34 ± 0.43	3.8	0.87	HST/WFC3-F160W	–	167 ± 15	11.13
S2F1-142 ⁴	03:06:36.51	00:03:01.0	1.386	3.04 ± 0.12	3.5	0.74	HST/NIC2-F160W	340^{120}_{-60}	347^{120}_{-60}	11.54

¹ Bezanson et al. (2013), ² van de Sande et al. (2013), ³ Belli et al. (2014), ⁴ Longhetti et al. (2014)

been removed by subtracting from each frame the following one in the dithering observing sequence. The sky-subtracted frames have been aligned and co-added. The final stacked spectra have been corrected for the response sensitivity function derived from the spectrum of the standard stars (FFEIGE110, GD71) observed in each of the 4 runs. Finally, we have applied a further correction to the relative flux calibration related to the x-position of the slit on mask (Lonoce et al. 2014). In Fig. 3 black lines show the 8-hours one dimensional spectra of our galaxies, not rebinned and unsmoothed.

For the velocity dispersion (σ) measurements we have adopted the Penalized Pixel-Fitting software (Cappellari & Emsellem 2004, pPXF) which derive the σ by fitting the continuum and the absorption features of the spectrum. We have derived the velocity dispersions from the unbinned spectra, weighting each pixel for a quantity proportional to its S/N, and adopting as templates a set of 33 synthetic stars selected from the high-resolution ($R \simeq 20000$) synthetic spectral library by Munari et al. (2005). The stars of the subsample have temperature $3500\text{K} < T < 10000\text{K}$, $0 < \log g < 5$, solar abundance and metallicity and are the same adopted by Cappellari et al. (2009) to derive the velocity dispersions of two ETGs at $z \sim 1.4$. A detailed description of the velocity dispersion measurements are provided in appendix D, together with extensive set of simulations aimed at testing the stability and accuracy of the measures, as well as their errors. In Table 4 we report the value of the velocity dispersion (σ) corrected for instrumental dispersion (~ 110 km/s) and their error (see Appendix B). Since data refer to 1" slit, the measured σ have to be considered within a radius of 0.5 arcsec. In Table 1 we report also σ_e , i.e. the velocity dispersion within the effective radius. We have scaled the measured σ to σ_e following Cappellari et al. (2006).

3.3. The evolution of structural and dynamical parameters of ultramassive dense ETGs: results

In the galaxy selection we have paid particular attention to the filter in which structural parameters were derived. The effective radii were derived in the F160W band for all the galaxies at $1.2 < z < 1.6$, in the F814W band for the sample at intermediate redshift range, and in the r band for the local SDSS galaxies, in order to sample approximately the same restframe band through all the redshift range we probe.

Figure 4 shows the distribution of ultramassive dense ETGs at $0 \lesssim z < 1.6$ in the plane defined by effective radius and stellar

mass. The six spheroids belonging to MUNICS sample (5 presented in Sec. 3.2 plus one by Longhetti et al. (2014)) are highlighted with black contours and we have highlighted with a blue point the ultramassive ETG of our high- z sample at $z = 1.91$. This galaxy is not included in the comparison with local ETGs.

Given the request of available velocity dispersion, the sample we have collected is clearly not complete and does not homogeneously cover the region of the size-mass plane occupied by dense galaxies. However, we have checked that the request of available velocity dispersion does not produce a bias against the most compact objects, i.e. that we are not missing the smallest ETGs at fixed stellar mass. In the Figure 5 the long-dashed black line is the lower boundary of the size-mass relation found by Belli et al. (2014) and van der Wel et al. (2014) (they are good agreement with each other). We notice that although not complete, our sample is not biased against dense ETGs, as expected since velocity dispersion measurements are more successful in dense systems.

In the left and right panels of Fig. 5 we plot the velocity dispersion of ultramassive dense ETGs a function of stellar mass and effective radius, respectively. The first thing that we may note is that all the ultramassive dense ETGs at high- z have an ultramassive dense counterpart in the local Universe with comparable structural and dynamical properties. Also the two most massive ($M_\star \gtrsim 3 \times 10^{11} M_\odot$) and densest ($\Sigma > 5000 M_\odot \text{pc}^{-2}$) high- z ETGs, whose parameters are offset with respect to the others high- z dense ETGs, have a counterpart. Their counterparts can be found among the local ultramassive dense galaxies belonging to the sample of SDSS galaxies with $\sigma > 350 \text{km/s}$ selected by Bernardi et al. (2008) (Fig. 5 open squares). Hence, Figure 6 shows that in local Universe there are ultramassive dense ETGs with effective radii and velocity dispersions comparable to those of equally massive and dense ETGs at $\langle z \rangle = 1.4$. At the same time, Fig. 5 shows that there are some local galaxies with $\sigma_e < 200$ km/s without an high- z counterpart. These ETGs populate in Fig. 4 the region immediately below the line at $\Sigma = 2500 M_\odot \text{pc}^{-2}$ with $10^{11} < M_\star < 2 \times 10^{11}$ where indeed no high- z galaxies fall. Actually, the sparse sampling of the high- z sample and its incompleteness, prevent us to assess whether the lack of low- σ ultramassive dense ETGs at high- z is real or not.

Just as exercise, in Fig. 5, with open circles, we show the displacement that high- z dense ETGs would show in the space (R_e, M_\star, σ_e) in the hypothesis that they evolve in size according to the relation $(1+z)^{-1.5}$ (i.e. a factor ~ 3 from $z \sim 1.4$ to $z = 0$ as found e.g. by Cassata et al. (2013), Cimatti et al. (2012), van der Wel et al. (2014)) and in σ according to the merging

Table 4. Our sample of high- z ETGs. *Column 1:* id number, *Column 2:* RA, *Column 3:* DEC, *Column 4:* redshift, *Column 5:* circularized effective radius in kpc, *Column 6:* Sersic index, *Column 7:* axis ratio, *Column 8:* velocity dispersion as measured within the 1'' aperture slit, *Column 9:* the range in which varies the offset factor σ_{off} to be applied to σ according to the simulation of Appendix B, *Column 10:* velocity dispersion as measured within the effective radius, *Column 11:* stellar mass derived with BC03 code and Chabrier IMF, *Column 12:* Vega magnitude in K band (Saracco et al. 2009)

Object	RA	Dec	z	R_e (kpc)	n	b/a	σ (km/s)	σ_{off} (km/s)	σ_e (km/s)	$\log(M_{\star,cha}/M_{\odot})$	K
S2F1-511	03:06:34.04	+00:02:30.9	1.267	2.09 ± 0.07	3.3	0.60	269	$[-4 \div 12]$	281^{+26}_{-40}	11.05	18.1 ± 0.1
S2F1-633	03:06:35.10	+00:04:43.6	1.297	2.59 ± 0.11	4.1	0.53	434	$[-24 \div -7]$	447^{+14}_{-19}	11.48	18.2 ± 0.1
S2F1-527	03:06:43.34	+00:02:44.8	1.331	1.57 ± 0.24	3.1	0.88	226	$[-16 \div 1]$	240^{+25}_{-28}	11.14	18.3 ± 0.1
S2F1-389	03:06:28.03	+00:00:31.6	1.406	2.10 ± 0.18	4.5	0.85	224	$[-30 \div -18]$	234^{+41}_{-41}	11.14	18.2 ± 0.1
S2F1-443	03:06:31.76	+00:01:13.4	1.910	3.36 ± 0.15	1.9	0.79	352	$[-21 \div 8]$	357^{+40}_{-64}	11.59	18.4 ± 0.1

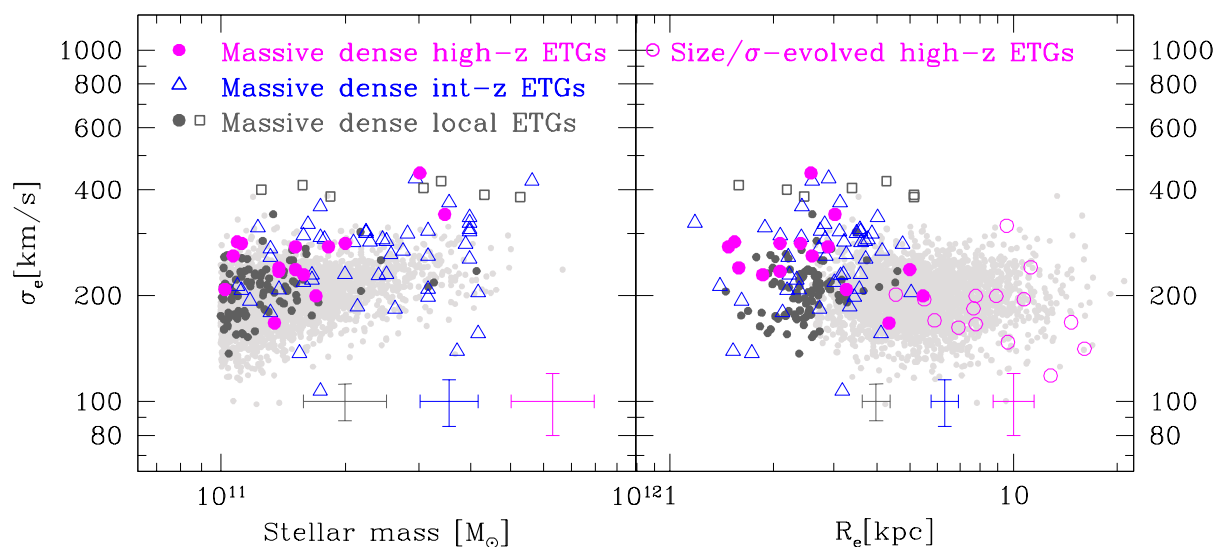


Fig. 5. Comparison between the structural and dynamical properties of ultramassive dense ETGs over the last ~ 10 Gyr. Magenta points are dense ETGs at $1.2 \lesssim z < 1.6$, open blue squares are dense ETGs at $0.3 \lesssim z < 0.9$, and local ETGs are dark grey small dots. Light grey points are the whole sample of local ETGs with $M_{\star} > 10^{11} M_{\odot}$, thus with no cut in mean stellar mass density. Grey open squares are the local ultramassive dense galaxies selected from the sample of local galaxies with velocity dispersion $> 350 \text{ km/s}$ by Bernardi et al. (2008), while open magenta circles are high- z ETGs evolved in size a factor ~ 3 as predicted by the relation $\langle R_e \rangle \propto (1+z)^{-1.5}$ and in σ according to the merger scenario by (Hopkins et al. 2009). In each panel, average error bars are reported. They are colour coded according to the sample they refer. For what concerns the high- z sample, we have found that on average $\delta_{R_e}/R_e \sim 11\%$, $\delta_{\sigma_e}/\sigma_e \sim 10\%$ (see Table 3 and 4), while we have assumed a typical uncertainty of 20% on M_{\star} . At intermediate redshift, $\delta_{R_e}/R_e \sim 10\%$, $\delta_{\sigma_e}/\sigma_e \sim 7\%$, and $\delta_{M_{\star}} = 0.10$ dex (see Saglia et al. 2010). In local Universe, $\delta_{M_{\star}} = 0.07$ dex (see Salim et al. 2007), $\delta_{\sigma_e}/\sigma_e \sim 10\%$, and we assume $\delta_{R_e}/R_e \sim 15\%$. For the error on local R_e we refer to La Barbera et al. (2010) which derive the structural parameters of SDSS galaxies on SDSS images using 2DPHOT. In fact, the errors on parameters are expected to be mainly driven by the characteristics of the images, and not by the software and/or procedure used.

scenario proposed by Hopkins et al. (2009). Thus, if all or most of the high- z ultramassive dense ETGs evolve in size (and σ_e) they have to be replaced by other ultramassive dense ETGs along the time to restore the population seen in the local Universe.

4. Discussion and Conclusions

We have investigated the mass accretion history of ultramassive dense ($M_{\star} > 10^{11} M_{\odot}$, $\Sigma > 2500 M_{\odot} \text{pc}^{-2}$) ETGs (elliptical and spheroidal galaxies, visually selected) over the last ~ 9 Gyr. We have addressed this topic by tracing the evolution of their comov-

ing number density and by comparing the structural (effective radius R_e and stellar mass M_{\star}) and dynamical (velocity dispersion σ_e) parameters of ultramassive dense ETGs from redshift ~ 1.6 to redshift ~ 0 .

In order to constrain the comoving number density ρ of ultramassive dense ETGs since $z = 1.6$, we have taken advantage of the MUNICS and GOODS-South surveys to probe the highest redshift range ($z > 1$), while we have used the COSMOS spectroscopic survey to cover the redshift range from $z = 1.0$ to $z = 0.2$. For the number density of ultramassive dense ETGs in the local Universe we have referred to the sample of local ETGs se-

lected from the SDSS DR4 by Thomas et al. (2010). We have found that the comoving number density follows the relation $\rho \propto (1+z)^{0.3 \pm 0.8}$, i.e., it decreases at most by 25% since $z=1.6$.

Our results are in good agreement with the other ones presented in literature (Carollo et al. 2013; Damjanov et al. 2015; Cassata et al. 2013; Valentinuzzi et al. 2010; Bezanson et al. 2013), with the only two exceptions concerning the estimates provided by Taylor et al. (2010a) at $z \sim 0$, and by van der Wel et al. (2014) at $0.2 < z < 1.5$ (in both cases our number densities are greater than that claimed by the authors). In the first case, we have shown that the main source of the observed discrepancy is the different definition of R_e used (semi-major axes SM_e obtained fitting a de Vaucouleur profile in Taylor’s paper versus circularized R_e obtained fitting a Sersic profile in our analysis). In the second case, we argue that the main reason of the drastic (\sim one order of magnitude) drop observed in the number density by van der Wel et al. (2014) can be ascribed to the procedure they adopted to derive the effective radius at 5000 Å and the usage of semi-major axis SM_e .

We have then investigated whether the ultramassive dense ETGs observed at high- z have a local counterpart, i.e. whether they are similar both in their structure (R_e and M_*) and kinematics (σ_e) to the low- z ones. To this aim, we have collected an homogeneous sample of ultramassive dense ETGs at $1.2 < z < 1.6$ with available R_e , M_* and σ_e . We have included in our final catalogue only the galaxies with clear elliptical morphology, effective radius derived in the F160W band fitting a Sersic profile and stellar masses estimated with BC03 models and a Chabrier IMF. The request of available velocity dispersion restricts the sample to 11 ETGs. For 4 ETGs out of 11 (plus one at $z = 1.91$) we have presented new unpublished VLT-FORS2 spectra and the measure of their velocity dispersions. For the intermediate redshift range ($0.2 < z < 0.9$) we refer to the sample of ETGs by Saglia et al. (2010), and to the sample of passive galaxies by Zahid et al. (2015), while as local reference we have adopted the complete sample of local ($0.063 < z < 0.1$) ETGs selected from the SDSS DR4 by Thomas et al. (2010). The comparison in the plane [R_e , M_* , σ_e] shows that all the ultramassive dense ETGs at $z = 1.4$, have a local counterpart with similar velocity dispersion, stellar mass and effective radius.

The two above evidences point toward two simple scenarios. In the last 9-10 Gyr, the vast majority ($\geq 70\%$, according to the number density) of ultramassive dense ETGs passively ages, leaving the bulk of the stellar mass, the kinematics, and the structure almost unchanged. In this case, the observed size growth of ultramassive ETGs has to be ascribed mostly to new born larger ETGs. The other possibility is that a significant fraction of high- z ultramassive dense ETGs migrates, through inside-out accretion, towards less dense systems, sustaining the mean size growth of spheroidal galaxies. Concurrently, the emergence of new ultramassive dense ETGs at lower redshift maintains the number density almost constant. We are not in the position to discriminate among the two possibilities, but some considerations deserve to be discussed.

A conventional approach to distinguish the real descendants from the newly formed spheroids (i.e. to discriminate among the two above scenarios) is to compare high redshift galaxies with old (on the basis of their luminosity weighted age LWA) low- z galaxies. However, this method does not take into account the evidence that despite the old global age, spheroidal galaxies often host very young stars (e.g. La Barbera et al. 2012). This population of young stars although has a negligible weight in term of total stellar mass (e.g. Tantaló & Chiosi 2004), can significantly lower the LWA. The direct consequence of this is that to

select local descendants through a cut in LWA can exclude part of spheroidal galaxies already in place at $z \sim 1.4$. As a further complication, most of the methods used to infer galaxies age are limited by the age-metallicity degeneracy and by the possible presence of the dust.

Considering these aspects, we have decided to investigate the distribution of local ultramassive dense ETGs in the $D_n(4000) - H_\delta$ plane. Actually, the $D_n(4000)$ index progressively increases with the age of the stellar population, while the strong absorption H_δ line arises in galaxies that have experienced a burst of star formation in the past 1-2 Gyr. Although both indices are metallicity sensitive, their combination is not so and, moreover, is largely insensitive to the dust-attenuation effects. In Fig. 6 we have reported the $D_n(4000)$ and H_δ values for our sample of 124 ultramassive dense local ETGs. For the spectral indices we have referred to the database provided by Kauffmann et al. (2003) for SDSS galaxies. The Figure shows that just $\sim 70\%$ (60%) of local ultramassive dense ETGs have $D_n(4000) \geq 1.9$ (1.95) (thus age ≥ 9 Gyr), so, on the basis of its age, only two out of three local ETGs should be considered a descendant of high- z compact ETGs. However, for each galaxy, Kauffmann et al. (2003) best-fitted the observed values of $D_n(4000)$ and H_δ with a grid of composite stellar population (CSP) models both with typical declining and bursty star formation history. From the best-fit model, they derived the fraction F of stellar mass formed in the last 2 Gyr, and provide both its median value and the 2.5 and 97.5 percentile of its likelihood distribution. Actually, all the galaxies in Fig. 6 have a median value of $F = 0$. However, in Fig. 6 we have colour coded the galaxies on the basis of the 97.5 percentile value of F ($F_{97.5}$). The reason of this choice is that more than the exact value of F , which can be susceptible to the input models grid and prior adopted in the fit, we are interested to investigate whether there is a non null probability to have a secondary (minor) event of star formation, that can drift the age estimate toward lower value. Interestingly, the vast majority of the galaxies with $D_n(4000) \geq 1.9$ (and less than 10% for galaxies with $D_n(4000) \geq 1.95$), $F_{97.5} = 0$. For the remaining galaxies of the sample with $D_n(4000) < 1.9$, their $F_{97.5}$ value is > 0 , thus there is a non null probability that they have experienced a burst of star formation in the last 2 Gyr. In this context, detailed studies on spectral features of passive galaxies (Lonoce et al. 2014) have shown that fitting the $D_n(4000)$ with a single CSP model with a declining star formation history returns age values that can be significantly (even $\geq 50\%$) lower than the values obtained with a SED fitting or obtained assuming a composite model made by an old component forming the bulk of the stellar mass, and a young stellar population contributing for just few % to the total stellar mass amount. If this is the case, the galaxies with $D_n(4000) < 1.9$ could be still considered descendant of high- z ETGs that experienced secondary and minor events of star formation at later epochs (see also Thomas et al. 2010). These events can have a drastic impact on the estimate of galaxy age, but do not alter significantly the stellar mass. Actually, Fig. 6 shows that the probability that a galaxy increases its stellar mass more than 20% in secondary events of star formation is extremely low.

This analysis, is not intended to be quantitative, but just to show that the treatment of the progenitor bias is really complex and that the mere selection of local descendants on the basis of the galaxy age obtained through the photometry fit or even through the more robust $D_n(4000)$ can provide at most a lower limit to the true number of local descendants. A more detailed analysis of the whole ensemble of the spectral features that are age and “star-formation history” sensitive (e.g. H_δ ; H+K,

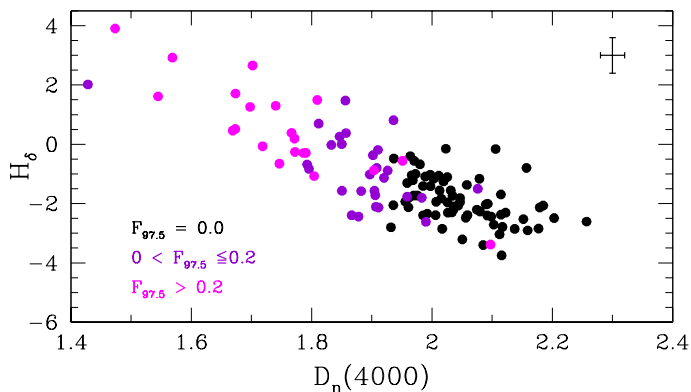


Fig. 6. The H_{δ} of ultramassive dense local ETGs versus their $D_n(4000)$ colour coded on the basis of the 97.5 percentile value of F , where F is the fraction of stellar mass formed in the last 2 Gyr.

$D_n(4000)$) is mandatory both in local and at intermediate redshift range, to track the real mass assembly history of ETGs.

Although not conclusive, the analysis of spectral features of local ETGs have shown that there is a non null probability that all the local dense ETGs are high- z descendants. Moreover, in the last years studies on the properties (number densities, masses, sizes, SFRs) of submillimeter galaxies (SMGs) have strengthen the possible evolutionary connection between these objects and dense high- z elliptical, with the first being the progenitors of the second ones (e.g. Barro et al. 2013, 2014; Toft et al. 2014). Nonetheless, these highly star forming galaxies are extremely rare at $z < 1$. If galaxies with, e.g., $D_n(4000) < 1.9$ are genuinely young ultradense systems (and not old galaxies which have experienced recent event of star formation), we should find the way to form them. The lack of progenitors for young dense ETGs, strengthen the hypothesis that the local compact massive galaxies are descendants of the high redshift ones.

Thus, more than one observational evidence would point toward the first of the two proposed scenarios according to which most ($\geq 75\%$) of the ultramassive dense ETGs observed at $z \sim 1.4$ have already completed their assembly. Although residual event of star-formation may occur, these cannot significantly modify neither the mass, nor the velocity dispersion, nor the typical dimension of the ultramassive dense galaxies already formed at $z \sim 1.4$. As far as the remaining 25% of dense ETGs possibly missing in the local universe, stochastic merger events could have transformed them in "non dense" systems ($\Sigma \leq 2500 M_{\odot} \text{pc}^{-2}$), contributing to the increase of the mean size and of the number density of the whole population of ultramassive ETGs at $z < 1.5$. Numerically, their contribution to the total number density of local ultramassive ETGs is $\sim 2 \times 10^{-5} \text{ gal/Mpc}^3$ (see Fig. 2). Actually, the number density of passive $M_{\star} > 10^{11} M_{\odot}$ galaxies increases from $\sim 10^{-4}$ to $5 \times 10^{-4} \text{ gal/Mpc}^{-4}$ from redshift 1.5 to $z \sim 0$ (Ilbert et al. 2010; Pozzetti et al. 2010; Brammer et al. 2011; Moustakas et al. 2013; Muzzini et al. 2013). Therefore, if the fraction of newly formed ultramassive dense ETGs is trascurabile, the eventual contribution of the size-evolved ultramassive dense ETGs to the mean size growth in term of number density is $\lesssim 5\%$.

Acknowledgements. We warmly thank the anonymous referee for his/her comments and suggestions which, in our opinion, have really improved the whole manuscripts. This work has received financial support from Prin-INAF

1.05.09.01.05 and is based on observations made with ESO Very Large Telescope under programme ID 085.A-0135A.

References

- Adelman-McCarthy, J. K., Agüeros, M. A., Allam, S. S., et al. 2006, *ApJS*, 162, 38
- Barro, G., Faber, S. M., Pérez-González, P. G., et al. 2013, *ApJ*, 765, 104
- Barro, G., Trump, J. R., Koo, D. C., et al. 2014, *ApJ*, 795, 145
- Belli, S., Newman, A. B., & Ellis, R. S. 2014, *ApJ*, 783, 117
- Bernardi, M. 2009, *MNRAS*, 395, 1491
- Bernardi, M., Hyde, J. B., Fritz, A., et al. 2008, *MNRAS*, 391, 1191
- Bezanson, R., van Dokkum, P., & Franx, M. 2012, *ApJ*, 760, 62
- Bezanson, R., van Dokkum, P., van de Sande, J., Franx, M., & Kriek, M. 2013, *ApJL*, 764, L8
- Bezanson, R., van Dokkum, P. G., Tal, T., et al. 2009, *ApJ*, 697, 1290
- Blanton, M. R. & Roweis, S. 2007, *AJ*, 133, 734
- Blanton, M. R., Schlegel, D. J., Strauss, M. A., et al. 2005, *AJ*, 129, 2562
- Brammer, G. B., Whitaker, K. E., van Dokkum, P. G., et al. 2011, *ApJ*, 739, 24
- Bruce, V. A., Dunlop, J. S., Cirasuolo, M., et al. 2012, *MNRAS*, 427, 1666
- Bruzual, G. & Charlot, S. 2003, *MNRAS*, 344, 1000
- Buitrago, F., Trujillo, I., Conselice, C. J., et al. 2008, *ApJL*, 687, L61
- Buitrago, F., Trujillo, I., Conselice, C. J., & Häußler, B. 2013, *MNRAS*, 428, 1460
- Calzetti, D., Armus, L., Bohlin, R. C., et al. 2000, *ApJ*, 533, 82
- Cappellari, M., Bacon, R., Bureau, M., et al. 2006, *MNRAS*, 366, 1126
- Cappellari, M., di Serego Alghieri, S., Cimatti, A., et al. 2009, *ApJL*, 704, L34
- Cappellari, M. & Emsellem, E. 2004, *PASP*, 116, 138
- Cappellari, M., Emsellem, E., Krajnović, D., et al. 2011, *MNRAS*, 413, 813
- Carollo, C. M., Bschorr, T. J., Renzini, A., et al. 2013, *ApJ*, 773, 112
- Carter, D., Goudfrooij, P., Mobasher, B., et al. 2008, *ApJS*, 176, 424
- Cassata, P., Giavalisco, M., Guo, Y., et al. 2011, *ApJ*, 743, 96
- Cassata, P., Giavalisco, M., Williams, C. C., et al. 2013, *ApJ*, 775, 106
- Chabrier, G. 2003, *PASP*, 115, 763
- Cimatti, A., Cassata, P., Pozzetti, L., et al. 2008, *A&A*, 482, 21
- Cimatti, A., Nipoti, C., & Cassata, P. 2012, *MNRAS*, 422, L62
- Daddi, E., Renzini, A., Pirzkal, N., et al. 2005, *ApJ*, 626, 680
- Damjanov, I., Abraham, R. G., Glazebrook, K., et al. 2011, *ApJL*, 739, L44
- Damjanov, I., Geller, M. J., Zahid, H. J., & Hwang, H. S. 2015, *ArXiv e-prints*
- Damjanov, I., Hwang, H. S., Geller, M. J., & Chilingarian, I. 2014, *ApJ*, 793, 39
- Damjanov, I., McCarthy, P. J., Abraham, R. G., et al. 2009, *ApJ*, 695, 101
- Davies, L. J. M., Driver, S. P., Robotham, A. S. G., et al. 2015, *MNRAS*, 447, 1014
- Drory, N., Feulner, G., Bender, R., et al. 2001, *MNRAS*, 325, 550
- Franx, M., van Dokkum, P. G., Schreiber, N. M. F., et al. 2008, *ApJ*, 688, 770
- Gargiulo, A., Saracco, P., Longhetti, M., La Barbera, F., & Tamburri, S. 2012, *MNRAS*, 425, 2698
- Giavalisco, M., Ferguson, H. C., Koekemoer, A. M., et al. 2004, *ApJ*, 600, L93
- Grogin, N. A., Kocevski, D. D., Faber, S. M., et al. 2011, *ApJS*, 197, 35
- Guo, Y., Giavalisco, M., Cassata, P., et al. 2011, *ApJ*, 735, 18
- Guo, Y., McIntosh, D. H., Mo, H. J., et al. 2009, *MNRAS*, 398, 1129
- Hopkins, P. F., Bundy, K., Murray, N., et al. 2009, *MNRAS*, 398, 898
- Hoyos, C., den Brok, M., Verdoes Kleijn, G., et al. 2011, *MNRAS*, 411, 2439
- Huertas-Company, M., Mei, S., Shankar, F., et al. 2013, *MNRAS*, 428, 1715
- Ilbert, O., McCracken, H. J., Le Fèvre, O., et al. 2013, *A&A*, 556, A55
- Ilbert, O., Salvato, M., Le Floch, E., et al. 2010, *ApJ*, 709, 644
- Jorgensen, I. & Chiboucas, K. 2013, *AJ*, 145, 77
- Jorgensen, I., Chiboucas, K., Toft, S., et al. 2014, *ArXiv e-prints*
- Kauffmann, G., Heckman, T. M., White, S. D. M., et al. 2003, *MNRAS*, 341, 33
- Keating, S. K., Abraham, R. G., Schiavon, R., et al. 2015, *ApJ*, 798, 26
- Koekemoer, A. M., Aussel, H., Calzetti, D., et al. 2007, *ApJS*, 172, 196
- Koekemoer, A. M., Faber, S. M., Ferguson, H. C., et al. 2011, *ApJS*, 197, 36
- Kormendy, J. 1982, *ApJ*, 257, 75
- Kormendy, J. & Illingworth, G. 1982, *ApJ*, 256, 460
- Kroupa, P. 2001, *MNRAS*, 322, 231
- La Barbera, F., de Carvalho, R. R., de La Rosa, I. G., et al. 2010, *MNRAS*, 408, 1313
- La Barbera, F., Ferreras, I., de Carvalho, R. R., et al. 2012, *MNRAS*, 426, 2300
- Longhetti, M., Saracco, P., Gargiulo, A., Tamburri, S., & Lonoce, I. 2014, *MNRAS*, 439, 3962
- Longhetti, M., Saracco, P., Severgnini, P., et al. 2007, *MNRAS*, 374, 614
- Lonoce, I., Longhetti, M., Saracco, P., Gargiulo, A., & Tamburri, S. 2014, *MNRAS*, 444, 2048
- Mancini, C., Daddi, E., Renzini, A., et al. 2010, *MNRAS*, 401, 933
- Mancini, C., Matute, I., Cimatti, A., et al. 2009, *A&A*, 500, 705
- Maraston, C. & Strömbäck, G. 2011, *MNRAS*, 418, 2785
- Marchesini, D., van Dokkum, P. G., Förster Schreiber, N. M., et al. 2009, *ApJ*, 701, 1765

Moresco, M., Pozzetti, L., Cimatti, A., et al. 2013, *A&A*, 558, A61
Moustakas, J., Coil, A. L., Aird, J., et al. 2013, *ApJ*, 767, 50
Munari, U., Sordo, R., Castelli, F., & Zwitter, T. 2005, *A&A*, 442, 1127
Muzzin, A., Marchesini, D., Stefanon, M., et al. 2013, *ApJ*, 777, 18
Newman, A. B., Ellis, R. S., Bundy, K., & Treu, T. 2012, *ApJ*, 746, 162
Newman, A. B., Ellis, R. S., Treu, T., & Bundy, K. 2010, *ApJL*, 717, L103
Peng, C. Y., Ho, L. C., Impey, C. D., & Rix, H. 2002, *AJ*, 124, 266
Poggianti, B. M., Calvi, R., Bindoni, D., et al. 2013a, *ApJ*, 762, 77
Poggianti, B. M., Moretti, A., Calvi, R., et al. 2013b, *ApJ*, 777, 125
Pozzetti, L., Bolzonella, M., Zucca, E., et al. 2010, *A&A*, 523, A13
Saglia, R. P., Sánchez-Blázquez, P., Bender, R., et al. 2010, *A&A*, 524, A6
Salim, S., Rich, R. M., Charlot, S., et al. 2007, *ApJS*, 173, 267
Saracco, P., Casati, A., Gargiulo, A., et al. 2014, *ArXiv e-prints*
Saracco, P., Longhetti, M., & Andreon, S. 2009, *MNRAS*, 392, 718
Saracco, P., Longhetti, M., & Gargiulo, A. 2010, *MNRAS*, L115+
Saracco, P., Longhetti, M., & Gargiulo, A. 2011, *MNRAS*, 412, 2707
Saracco, P., Longhetti, M., Severgnini, P., et al. 2005, *MNRAS*, 357, L40
Sargent, M. T., Carollo, C. M., Lilly, S. J., et al. 2007, *ApJS*, 172, 434
Scarlata, C., Carollo, C. M., Lilly, S., et al. 2007, *ApJS*, 172, 406
Severgnini, P., Della Ceca, R., Braitto, V., et al. 2005, *A&A*, 431, 87
Shen, S., Mo, H. J., White, S. D. M., et al. 2003, *MNRAS*, 343, 978
Simard, L., Mendel, J. T., Patton, D. R., Ellison, S. L., & McConnell, A. W. 2011, *ApJS*, 196, 11
Stott, J. P., Collins, C. A., Burke, C., Hamilton-Morris, V., & Smith, G. P. 2011, *MNRAS*, 414, 445
Strauss, M. A., Weinberg, D. H., Lupton, R. H., et al. 2002, *AJ*, 124, 1810
Szomoru, D., Franx, M., Bouwens, R. J., et al. 2011, *ApJ*, 735, L22
Szomoru, D., Franx, M., & van Dokkum, P. G. 2012, *ApJ*, 749, 121
Tamburri, S., Saracco, P., Longhetti, M., et al. 2014, *ArXiv e-prints*
Tantalo, R. & Chiosi, C. 2004, *MNRAS*, 353, 405
Taylor, E. N., Franx, M., Brinchmann, J., van der Wel, A., & van Dokkum, P. G. 2010a, *ApJ*, 722, 1
Taylor, E. N., Franx, M., Glazebrook, K., et al. 2010b, *ApJ*, 720, 723
Thomas, D., Maraston, C., Schawinski, K., Sarzi, M., & Silk, J. 2010, *MNRAS*, 404, 1775
Thomas, D., Steele, O., Maraston, C., et al. 2013, *MNRAS*, 431, 1383
Toft, S., Smolčić, V., Magnelli, B., et al. 2014, *ApJ*, 782, 68
Toft, S., van Dokkum, P., Franx, M., et al. 2007, *ApJ*, 671, 285
Treu, T., Stiavelli, M., Møller, P., Casertano, S., & Bertin, G. 2001, *MNRAS*, 326, 221
Trujillo, I., Cenarro, A. J., de Lorenzo-Cáceres, A., et al. 2009, *ApJ*, 692, L118
Trujillo, I., Conselice, C. J., Bundy, K., et al. 2007, *MNRAS*, 382, 109
Trujillo, I., Feulner, G., Goranova, Y., et al. 2006, *MNRAS*, 373, L36
Valentinuzzi, T., Fritz, J., Poggianti, B. M., et al. 2010, *ApJ*, 712, 226
van de Sande, J., Kriek, M., Franx, M., et al. 2013, *ApJ*, 771, 85
van der Wel, A., Bell, E. F., Häussler, B., et al. 2012, *ApJS*, 203, 24
van der Wel, A., Franx, M., van Dokkum, P. G., et al. 2014, *ApJ*, 788, 28
van der Wel, A., Holden, B. P., Zirm, A. W., et al. 2008, *ApJ*, 688, 48
van der Wel, A., Rix, H.-W., Wuyts, S., et al. 2011, *ApJ*, 730, 38
van Dokkum, P. G., Franx, M., Kriek, M., et al. 2008, *ApJ*, 677, L5
Wake, D. A., van Dokkum, P. G., & Franx, M. 2012, *ApJL*, 751, L44
Windhorst, R. A., Cohen, S. H., Hathri, N. P., et al. 2011, *ApJS*, 193, 27
Zahid, H. J., Damjanov, I., Geller, M. J., & Chilingarian, I. 2015, *ApJ*, 806, 122
Zirm, A. W., van der Wel, A., Franx, M., et al. 2007, *ApJ*, 656, 66

Appendix A: Testing the reliability of R_e and M_* for local SDSS ETGs

Appendix A.1: Effective radius of local SDSS ETGs

The effective radius for SDSS galaxies has been derived by many authors adopting different methods (e.g. 1D fit with the NYU-VAC pipeline by Blanton et al. (2005), 2D fit with GALFIT by Simard et al. (2011) and Guo et al. (2009)) and it is not straightforward to assess which analysis provides the more accurate estimate of the parameter. In fact, all these works have estimated the R_e on SDSS images (PSF-FWHM = 1.4" in r band, pixel size = 0.396"/px, i.e. ~ 0.56 kpc/px at $z = 0.075$), and thus the central region of the light profile (much sensitive to the Sersic index) of a typical ultramassive dense ETG is sampled by just 3-4 px in the redshift range we probe. Based on this evidence, to test the accuracy of the R_e we have used in this work, we have compared the estimate of the effective radius derived by Blanton et al. (2005) on SDSS images, with those obtained using HST optical images (FWHM $\approx 0.12''$, pixel size 0.05"/px). We

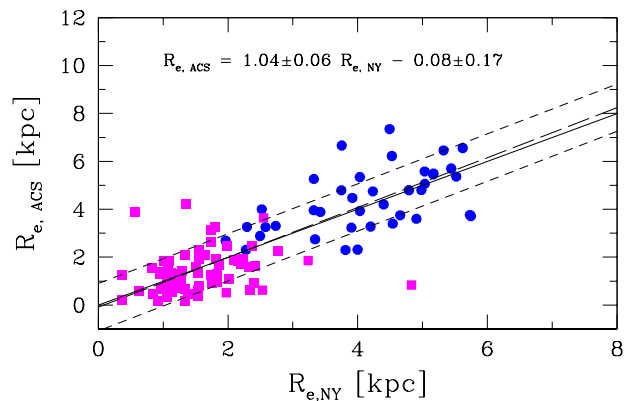


Fig. A.1. Effective radius measured on F814W/HST images for galaxies at $0.1 < z < 0.4$ (blue points) and for galaxies in Coma cluster (magenta squares) compared with the estimates obtained on SDSS images by Blanton et al. (2005) in r -band, for galaxies at $0.1 < z < 0.4$, and in i -band images for Coma galaxies. Solid line is the 1:1 correlation, long-dashed line is the best fit relation obtained with a sigma clipping algorithm, and dashed lines indicate the 1σ deviation from the best fit.

have used the Canadian Astronomy Data Centre⁵ to find ACS-HST images in the F775W/F814W/F850LP/ filter for the 124 ultramassive dense ETGs of our sample, but, unfortunately, none of them has HST optical counterpart.

Given this, we have collected from literature a sample of galaxies included in the Blanton's catalogue with R_e estimated also on HST images. We firstly refer to the COSMOS catalogue described in section 2.2. In figure A.1 the R_e of galaxies at $0.1 < z < 0.4$ measured on HST/ACS-F814W images ($\sim r$ -band rest-frame) by Sargent et al. (2007) is reported versus the R_e (r band) taken from Blanton's release (blue points). The match between the two releases do not include galaxies with R_e smaller than 2 kpc, hence, in order to investigate the reliability of Blanton estimates even at lower effective radii, we integrate the sample with galaxies taken from the ACS-Coma Cluster Survey (Carter et al. 2008). The effective radius of Coma galaxies were measured on the F814W images (exposure time ~ 1400 s) with GALFIT (Hoyos et al. 2011) and in Fig. A.1 is compared with the i -band SDSS R_e . The range of R_e covered by the two samples ($1 \text{ kpc} \lesssim R_e \lesssim 6 \text{ kpc}$) is very similar that covered by our sample of ultramassive dense local ETGs. The Figure shows that in the range of radius of our ultramassive dense ETGs ($1 \text{ kpc} \lesssim R_e \lesssim 6 \text{ kpc}$), the estimates by Blanton agree with that measured on HST images ($R_{e,HST} = 1.03 \pm 0.08 R_{e,NY} + 0.06 \pm 0.24$).

Appendix A.2: Stellar mass of local SDSS ETGs

SDSS galaxies are provided with different estimates of stellar masses. In our analysis we have decided to adopt the stellar masses derived through the SED fitting for consistency with high and intermediate redshift stellar mass estimates. In order to show that our conclusions are not affected by our choice of M_* , in this Appendix we compare two different estimates of this quantity in order to assess the consistency of the measures, at least in the range of values we are interested in.

⁵ (<http://www2.cadc-ccda.hia-ihp.nrc-cnrc.gc.ca/en/search/?collection=CFHTMEGAPIPE&noexec=true#queryFormTab>)

In the left panel of Fig. A.2 we plot the stellar mass derived through the fit of the multiband photometry (used in this paper, $M_{\star,photo}$) versus that obtained fitting the spectral indices ($M_{\star,index}$, Kauffmann et al. 2003).

The figure shows that for the bulk of local ETGs with $M_{\star,photo} > 10^{11} M_{\odot}$ the two estimates agree well, but few percent of them significantly deviate from the main correlation. We have identified these outliers, in figure represented by squares, as those galaxies at 3 sigma from the best-fit relation derived with a sigma clipping algorithm. We notice that a significant fraction of outliers below the relation has $M_{\star,photo} > 10^{11} M_{\odot}$, while $M_{\star,index} < 10^{11} M_{\odot}$. Among these ultramassive outliers, we have highlighted with open blue squares those with $\Sigma > 2500 M_{\odot} pc^{-2}$, i.e. those included in local sample of ultramassive dense local ETGs. To discriminate for these ultramassive outliers the stellar mass estimate more realistic, in the central panel we plot the the velocity dispersion derived from the virial theorem (σ_{vir})

$$\sigma_{vir} = \sqrt{GM_{\star,photo}/\beta R_e}, \quad (A.1)$$

where G is the gravitational constant and $\beta = (8.87 - 0.831 \times n + 0.0241 \times n^2)$ following Cappellari et al. (2006), versus the measured one (σ_{dr7}). For the velocity dispersions of local ETGs we have referred to the DR7 σ (see Thomas et al. (2013) for more tests on the reliability of DR7 σ estimates).

The majority of ultramassive outliers deviate from the general trend and in particular at fixed σ_{dr7} , σ_{vir} should be lower. This suggests that the $M_{\star,photo}$ for these galaxies are overestimated. As further confirmation, in the bottom panel we plot σ_{dr7} versus σ_{vir} but with the last quantity derived from the $M_{\star,index}$ estimates. We observe that in this case, the ultramassive outliers follow the main relation.

In fact, most of the ultramassive outliers despite having $M_{\star,photo} > 10^{11} M_{\odot}$ have $M_{\star} < 10^{11} M_{\odot}$, and thus we will exclude them from our sample of local ultramassive dense ETGs.

Appendix B: Insights on the impact of R_e definition on the samples of local dense galaxies.

In Sec. 2.5.1, we have shown that the number of local massive dense galaxies is drastically dependent on the R_e used. In particular, we have shown that in the spectroscopic SDSS-DR7 release, the number of galaxies with $M_{\star} > 10^{11} M_{\odot}$, $\log(R_e/kpc) < 0.56 \times (\log(M_{\star}/M_{\odot}) - 9.84) - 0.3$, and $^{0.1}(u-r) > 2.5$ is ~ 10 if semi-major axis obtained fitting a de Vaucouleur profile ($SM_{e,dv}$) is used and rises up to ~ 190 if circularized de Vaucouleur one ($R_{e,dv}$) is used instead. Hereafter, for sake of convenience, we refer to this last sample as "circularized sample". This implies that circularization (hence the axis ratio b/a) has a huge impact on the selection of the sample. In order to better visualize the impact of the b/a ratio on the selection of the samples, we have plotted in the size-mass plane the galaxies of the circularized sample with reliable stellar mass (see Sec. 2.5.1) using for each galaxy its semi-major axis $SM_{e,dv}$. We have color coded the galaxies according to their b/a ratio. The solid line indicates the relation $\log(R_{e,dv}/kpc) = 0.56 \times (\log(M_{\star}/M_{\odot}) - 9.84) - 0.3$. As expected, the Figure shows that ~ 10 galaxies have $\log(R_{e,dv}/kpc) < 0.56 \times (\log(M_{\star}/M_{\odot}) - 9.84) - 0.3$, while all the others lie above the line, with a b/a ratio that progressively decreases with the distance from the solid line, down to $b/a \approx 0.3$. In the central panel of Fig. B.1 we have reported the distribution of the axis ratio b/a for the same sample of galaxies. Half of the sample has $b/a < 0.5$, and this is the main reason of the drastic difference

between the samples selected using circularized R_e , and semi-major axis SM_e . The leftmost panel of Fig. B.1 also show that only the galaxies with $b/a \gtrsim 0.8-0.9$ are all included in both samples, and this is the main reason why even if our ultramassive dense ETGs are expected to be mostly roundish systems, i.e. objects for which their semi-major axes should be similar to their R_e , Taylor et al. do not selected them in their sample. In fact, we have checked that only the $\sim 5\%$ (6 galaxies) of ETGs in our sample has $b/a > 0.8$, and are exactly those satisfying the Taylor's conditions.

Finally, in Sec. 2.5.1 we have found that the number of local galaxies with $M_{\star} > 10^{11} M_{\odot}$, $\log(R_e/kpc) < 0.56 \times (\log(M_{\star}/M_{\odot}) - 9.84) - 0.3$, $^{0.1}(u-r) > 2.5$ still increases if circularized Sersic R_e are used (in particular, just the $\sim 45\%$ of the galaxies are included in the sample selected using circularized de Vaucouleur R_e). This result, as claimed in Sec. 2.5.1, is expected, since dense galaxies are known to have Sersic index lower than 4. In the right panel of Fig. B.1 we have reported the distribution of the Sersic index n for the local dense galaxies selected using the Taylor et al.'s cut and circularized Sersic R_e : more than 80% of the galaxies has $n < 4$. There is also a tail of galaxies with Sersic index lower than 2. This is mainly due to the fact that galaxies are selected with a color cut, and it is known that there is a non negligible fraction of red disk. Actually, as comparison, the magenta histogram in the right panel of Fig. B.1 shows the distribution of the Sersic index for our sample of ultramassive dense ETGs. It is nice to observe how the tail at $n < 2$ disappears (we remind that no selection on the Sersic index is imposed *a priori* to the local sample of ETGs, as well as to no other sample used in our analysis), strengthening the robustness of the visual classification in selecting spheroidal galaxies.

Appendix C: The effect of the extrapolation on the size measurements

In Section 2.5.3, we have shown that the extrapolation of the size of a galaxy via the Eq. 2 by van der Wel et al. (2014), has an impact on the number of dense galaxies. In this Appendix, we want to deepen this aspect. In Figure C.1, for the two bins of redshift $0.5 < z < 0.7$, and $0.7 < z < 0.9$, we have reported the distribution of $\text{Log}(SM_{e,5000\text{\AA}meas}/SM_{e,5000\text{\AA}der})$ for a sample of elliptical galaxies, where $SM_{e,5000\text{\AA}meas}$ is the semi-major axis at 5000 Å restframe measured directly on images, and $SM_{e,5000\text{\AA}der}$ is the one derived from $SM_{e,F125W}$ using the Eq. 2 by van der Wel et al. (2014). For the galaxies at $0.5 < z < 0.7$, we refer to a subsample of COSMOS ellipticals. In details, for the $SM_{e,5000\text{\AA}meas}$ values we refer to the measurements by Sargent et al. (2007) on the F814W-band images and discussed in Sec. 2.2, while for the $SM_{e,F125W}$ values we have considered the estimates by van der Wel et al. (2012). We have crossmatched the two catalogues, and have selected only elliptical (ZEST-type = 1) galaxies with $M_{\star} > 10^{10} M_{\odot}$. For the galaxies at $0.7 < z < 0.9$, we have considered a sample of elliptical galaxies in the GOODS-South field. For the $SM_{e,5000\text{\AA}meas}$ values we have used our sample of ETGs on GOODS-South (Tamburri et al. 2014) with SM_e derived on F850LP images (briefly described in Sec. 2.1), and for the $SM_{e,F125W}$ measurements we have considered the catalogue by van der Wel et al. (2012). At $0.5 < z < 0.7$, $SM_{e,5000\text{\AA}der}$ overestimates the $SM_{e,5000\text{\AA}meas}$ by a factor -0.08 dex (median value), and in particular for more than 80% of the galaxies $SM_{e,5000\text{\AA}meas}/SM_{e,5000\text{\AA}der} < 1$. At $0.7 < z < 0.9$, where the correction is extrapolated over a shorter wavelength range, this fraction lowers to $\sim 65\%$, and the median value is -0.02 . The two

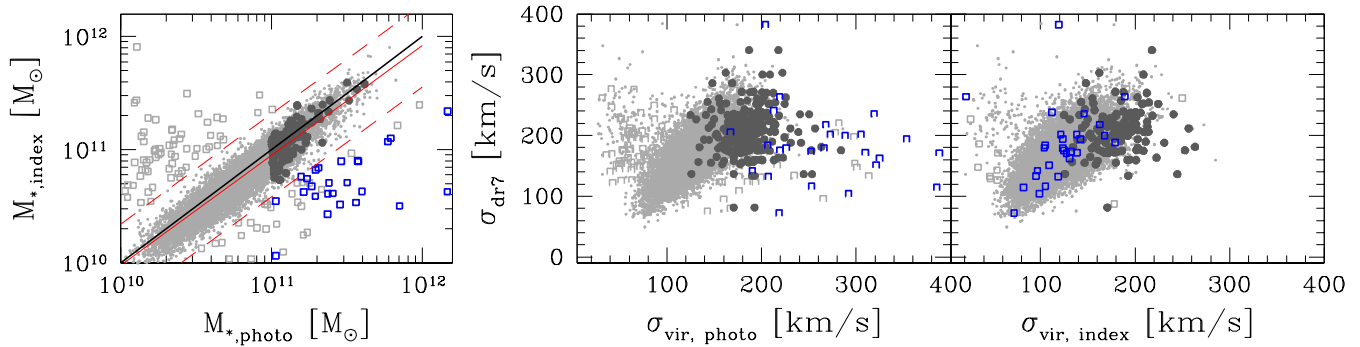


Fig. A.2. *Left panel:* the stellar mass derived through the fit of the multiband photometry (used in this paper, $M_{\star, \text{photo}}$) versus that obtained fitting the spectral indices ($M_{\star, \text{index}}$, Kauffmann et al. 2003) for local ETGs at $0.05 < z < 0.1$ (light grey points). Black solid line is the 1:1 correlation, while red line is the best-fit relation and red-dotted curves are the 3σ lines. All the points at $> 3\sigma$ are marked as open squares. Among these outliers, blue ones are those having $M_{\star} > 10^{11} M_{\odot}$, and $\Sigma > 2500 M_{\odot} \text{pc}^{-2}$, i.e. nominally included in local sample of ultramassive dense local ETGs. Dark grey points are the remaining part of the ultramassive dense local ETGs. *Central panel:* the measured velocity dispersion (σ_{dr7}) versus the velocity dispersion derived from the virial theorem assuming as mass the $M_{\star, \text{photo}}$ values ($\sigma_{\text{vir, photo}}$). *Right panel:* the same of central panel but with σ_{vir} derived assuming the $M_{\star, \text{index}}$ values.

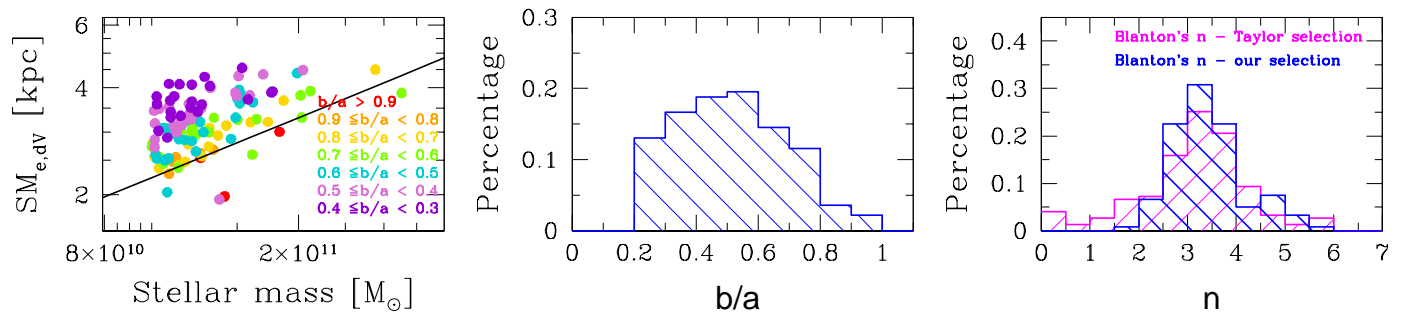


Fig. B.1. *Left panel:* The sample of local dense galaxies, selected using the Taylor et al.'s cuts and circularized de Vaucouleur radius $R_{e, \text{dv}}$, plotted in the size-mass plane using their semi-major de Vaucouleur axis $SM_{e, \text{dv}}$. Galaxies are color coded according to their b/a ratio, as declared in the labels. Solid line indicates the $\log(R_{e, \text{dv}}/\text{kpc}) = 0.56 \times (\log(M_{\star}/M_{\odot}) - 9.84) - 0.3$ relation. *Central panel:* The distribution of the axis ratio b/a for the same galaxies in the left-panel. Histogram counts are normalized to unity. *Right panel:* The distribution of the Sersic index n of local dense galaxies selected using Taylor et al.'s cuts, and circularized Sersic radius (blue histogram). Histogram counts are normalized to unity. Magenta histogram is the distribution of the Sersic index for our sample of ultramassive dense ETGs.

samples of galaxies at $0.5 < z < 0.7$ and $0.7 < z < 0.9$ do not have exactly the same distribution in stellar mass and this can alter the relative comparison of their $SM_{e, 5000\text{\AA} \text{meas}}/SM_{e, 5000\text{\AA} \text{der}}$ values. However, we have checked that the ratio $SM_{e, F850LP}/SM_{e, F125W}$ and $SM_{e, F850LP}/SM_{e, F125W}$ does not depend on stellar mass, as stated by van der Wel et al. (2014). Although test on more statistically significant samples would be necessary to be conclusive, the Fig. C.1 shows that an average variation of SM_e with λ (as assumed in the Eq. 2 by van der Wel) could not account for the variety of stellar populations in elliptical galaxies at high redshift (see e.g. Guo et al. 2011; Gargiulo et al. 2012), and this should be taken in mind in the interpretation and comparison of the achieved results.

Appendix D: Velocity dispersion measurements at $z \sim 1.4$

Fig. 3 shows the FORS2 spectra of the five galaxies of our high- z sample. As expected from the redshift estimates based on the continuum shape provided by AMICI spectra in the framework of the MUNICS survey, for the four galaxies at $z \lesssim 1.4$ (ID 511, 633, 527, 389) we have detected many absorption features (e.g. CN(3833Å), the CaII K and H (3933+3968Å), blue lines) besides the 4000Å break. We notice that the ETG 527, whose elliptical morphology is confirmed by the HST image and surface brightness profile (see Fig. 1), clearly shows the O_2 emission line at 3727Å. We exclude that the presence of this emission line is due to AGN activity. In fact, the 5 ETGs of our sample were observed with XMM observations and only the source 443 has an X-ray detection (Severgnini et al. 2005). For galaxy 443 we have detected, as expected, the MgII absorption feature. However, we

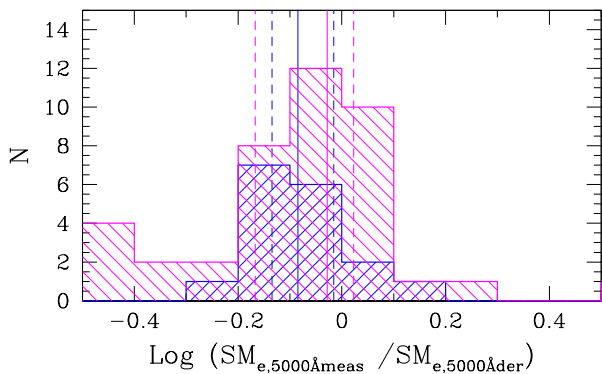


Fig. C.1. The distribution of the $SM_{e,5000\text{\AA}meas}/SM_{e,5000\text{\AA}der}$ ratio as function of the redshift. $SM_{e,5000\text{\AA}meas}$ is the semi-major axis at 5000\AA restframe measured directly on images, while $SM_{e,5000\text{\AA}der}$ is the same quantity, but inferred from F125W-band images using the Eq. 2 van der Wel et al. (2014). Blue histogram refers to ETGs at $0.5 < z < 0.7$, while magenta one to ETGs at $0.7 < z < 0.9$. Solid lines are the median values of the distributions and dotted ones are the 25 and 75 percentile.

notice that the detection of this absorption line fixes the redshift of this galaxy at $z=1.91$ slightly higher than the value originally estimated from the AMICI continuum ($z = 1.70 \pm 0.05$). In Table 4 we report the values of the redshifts for the five galaxies of our sample.

The tool pPXF we have adopted to derive the velocity dispersion describes the line of sight velocity distribution (LOSVD) as a Gauss+Hermite polynomial to take into account possible deviation of the line profile from a pure Gaussian shape. Following the prescription of the pPXF documentation, we have run simulations to define the value of the BIAS parameter, a penalty term which biases the solution towards a Gaussian shape if the higher moments of Hermite polynomial are not constrained from the data, and have found that for our galaxies it ranges between 0.1 and 0.2, in agreement with Cappellari et al. (2011).

Once fixed the BIAS level, we have measured the velocity dispersion by means of a weighted fit and adopting as templates a set of synthetic stars (see Sec. 3.1). To check for possible dependence of the σ estimate on the selected templates, we have repeated the measure adopting a set of BC03 models with solar metallicity, $\tau = 0.1$ Gyr and varying age. We have found σ values perfectly comparable (differences $< 5\%$) with those obtained with Munari's stars. For clarity, the values reported in this paper and used in the analysis refer to σ estimates derived adopting the set of stars as templates.

We have included in the fitting function both additive and multiplicative polynomials to take into account possible residual template mismatch, and eventual sky subtraction and spectral calibration errors. We have verified the stability of our measures varying the degree (up to 6) of the two set of polynomials and have found that the detected variations in the estimates of velocity dispersion are lower than 3%, well within 1σ error bar.

Four out of five ETGs of our sample have spectra covering the restframe wavelength range $\sim [0.3 - 0.43]\mu\text{m}$, thus including the 4000\AA break and many absorption features among which Ca H+K. In the past, several analysis have reported that the inclusion of the H+K features lead to an overestimate of the σ value, up to a factor of $\sim 20\%$ (Kormendy

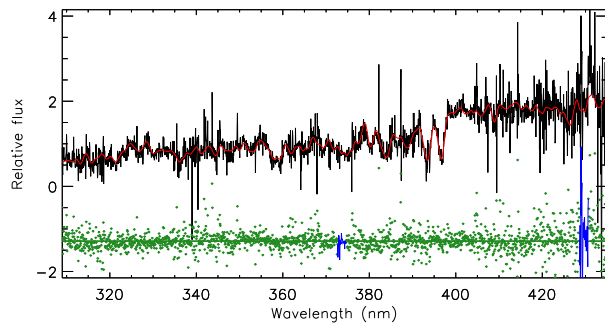


Fig. D.1. An example of the galaxy spectrum template (black line) we have constructed for the real galaxy S2F1-633. Red line is the best-fit model, while green points are the residuals.

1982; Kormendy & Illingworth 1982). These lines are intrinsically broad ($\sim 5\text{\AA}$), and in addition, the CaH line at 3968\AA is blended with H ϵ at 3969\AA . Moreover, error in the fitting the steep continuum gradient at 4000\AA could produce a template mismatch. All these factors can invalidate the measured dispersions. Nonetheless the real impact of this feature on the σ estimates is not quantifiable a priori (e.g. Treu et al. 2001; van de Sande et al. 2013), thus we have organized a set of simulations to test the reliability of our velocity dispersion measurements.

Briefly, for each galaxy of our sample, we have created four model galaxy spectra starting from a simple stellar population model from Maraston & Strömbäck (2011) with solar metallicity and age 2, 3, 4, 5 Gyr. We have redshifted the spectra to the galaxy redshift, degraded them to the dispersion of real spectrum ($\sim 55\text{ km/s}$ per pixel) and added to them, pixel-by-pixel, a fake noise randomly extracted by the real one. These template spectra have been convoluted with a Gauss+Hermite LOSVD with the h_3 and h_4 Hermite's moment equal to those measured on real spectrum and velocity dispersion (σ_{in}) varying in the range $\sim [200-500]\text{ km/s}$ over 500 steps. We have fixed the line-of sight velocity V to zero. As example, in Fig. D.1 we report a galaxy spectrum template we have constructed for the galaxy S2F1-633, with velocity dispersion 400 km/s (black line). With the same star templates used on real spectra, we have measured their velocity dispersions (σ_{out}) assuming as fitting function a Gauss+Hermite polynomial. In Fig D.2, D.3, D.4, D.5, D.6 we present the results of the simulations for the galaxy S2F1-511, S2F1-633, S2F1-527, S2F1-389, S2F1-443.

The results we have obtained show that, irrespective of the stellar population properties, for all the galaxies of our sample, fitting a Gauss+Hermite polynomial over the whole wavelength range covered by our spectra, with a penalty BIAS ≈ 0.1 , is the best choice to recover the intrinsic value of velocity dispersions. The same set of simulations for the galaxy 443 shows the feasibility of extracting a reliable estimate of velocity dispersion from spectrum covering the blue wavelength range shortward the 4000\AA in agreement with what found by Cappellari et al. (2009).

In facts, the difference $\sigma_{out} - \sigma_{in}$ shows a slight offset which is always lower than the dispersion of the real spectrum ($\sim 55\text{ km/s}$ per pixel). The exact magnitude of the offset depends on the age and metallicity of the stellar population. We verified that the amount of the offset is not reduced excluding from the fit the region around the Ca H+K features, as done by

Kormendy & Illingworth (1982), for this reason we have decided to include this part of the spectrum in our fit.

Moreover, our simulations have shown that for the σ we expect for our galaxies, the median value of the offset between σ_{in} and σ_{out} ($\sigma_{off,median} = \sigma_{out} - \sigma_{in}$) depends on the age and metallicity of the input template, but is always smaller than the statistical error on measured velocity dispersion. In Table 4 we have reported, for each galaxy, the minimum and maximum value of $\sigma_{off,median}$ we have found in the 6 sets of simulations when σ_{out} is equal to the value we have measured on real spectrum. From the Table appears that the offset is never greater than 30 km/s and can be both positive and negative. Given these two aspects, and our uncertainty on stellar population properties, mostly on metallicity, we have decided to not correct our measures for this offset, since we are not able to properly quantify its magnitude. Nonetheless, we note that our results would not change if we corrected the velocity dispersion of each galaxy for the maximum value of its offset.

The errors on velocity dispersion reported in Table 1 are the 25th and 75th percentile of the distributions of σ_{off} estimated at σ_{out} equal to the velocity dispersion measured on real spectrum. Among the different set of simulations, the quoted errors are extracted from the simulation performed starting from a simple stellar population model with solar metallicity and age equal to that obtained from the fit of the observed SED. However, although the value of the offset is slightly dependent on the stellar population properties, its scatter not.

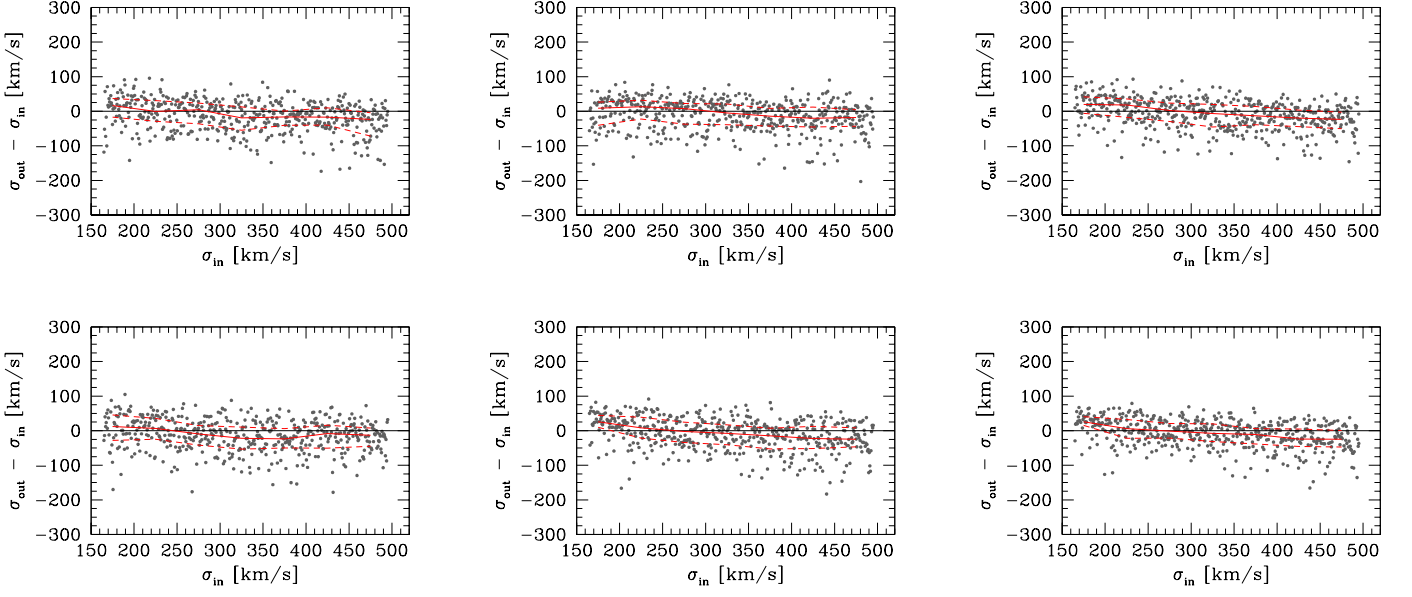


Fig. D.2. *Top row:* The difference between the velocity dispersion measured (σ_{out}) and that provided as input (σ_{in}) in the model as function of σ_{in} for galaxy S2F1-511. The template adopted in the simulation have solar metallicity and age 2, 4, 5 Gyr from left to right. It is evident that the age of stellar population do not affect our measurements. *Bottom row:* Same of top row for the template with age 3 Gyr and sub-solar, solar and super-solar metallicity from left to right. The three panels show that our uncertainty on stellar metallicity does not compromise our σ estimates. Red solid line is the median of the distribution, while dashed lines are the 25th and the 75th percentile.

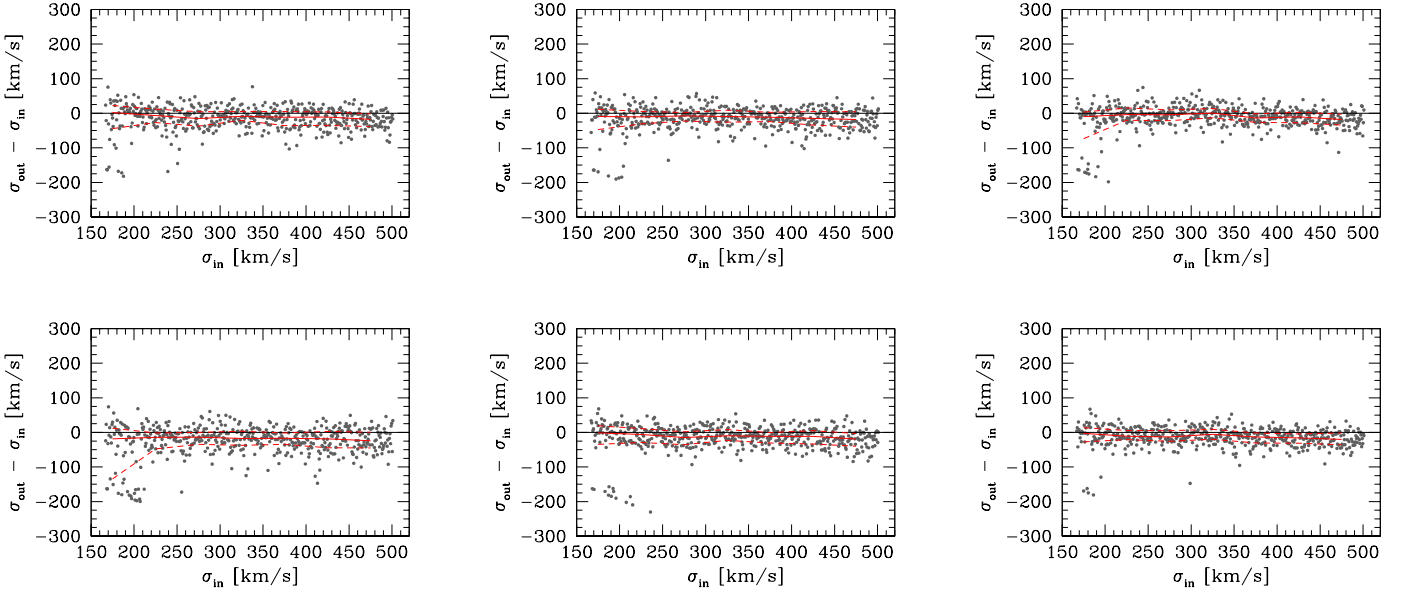


Fig. D.3. The same as Fig. D.2 for galaxy S2F1-633.

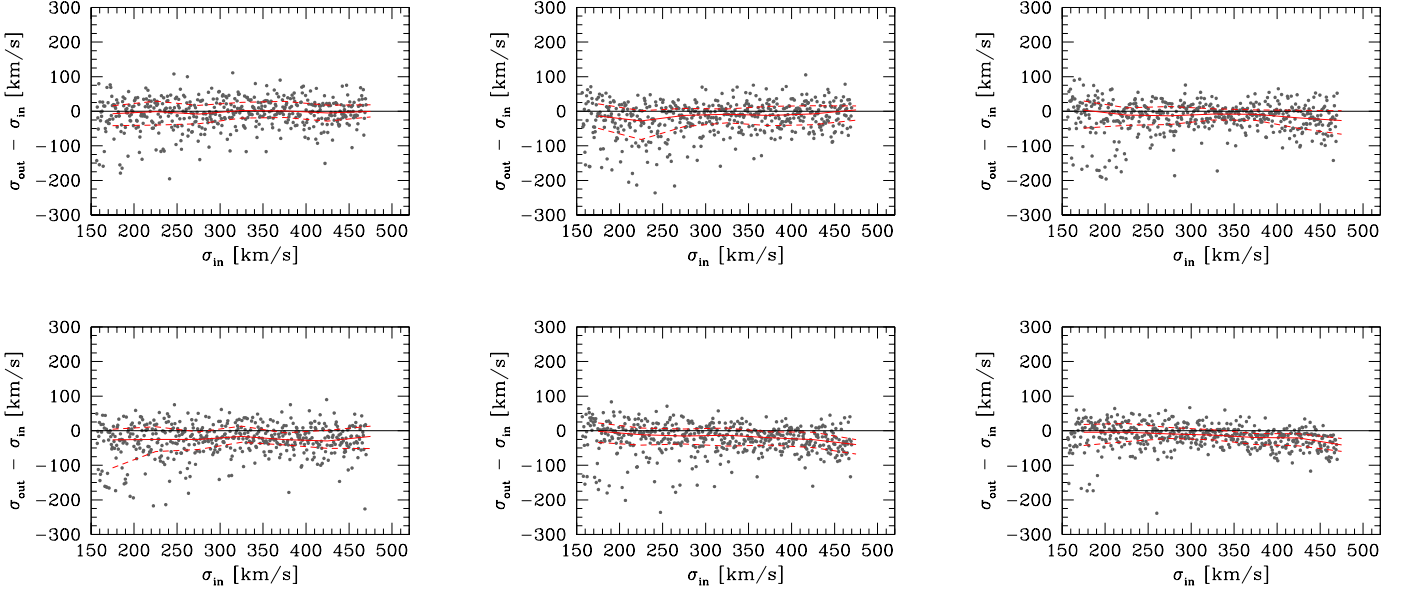


Fig. D.4. The same as Fig. D.2 for galaxy S2F1-527. Given the spectrum and the SED fitting of this ETG, which both suggest a very young age for its stellar population, in the simulation of this galaxy we have adopted as galaxy template simple stellar population templates with solar metallicity and age 0.5, 1, 2 Gyr (upper panels, from left to right) and stellar population templates with an age of 3 Gyr and sub-solar, solar, and super-solar metallicity (lower panels, from left to right).

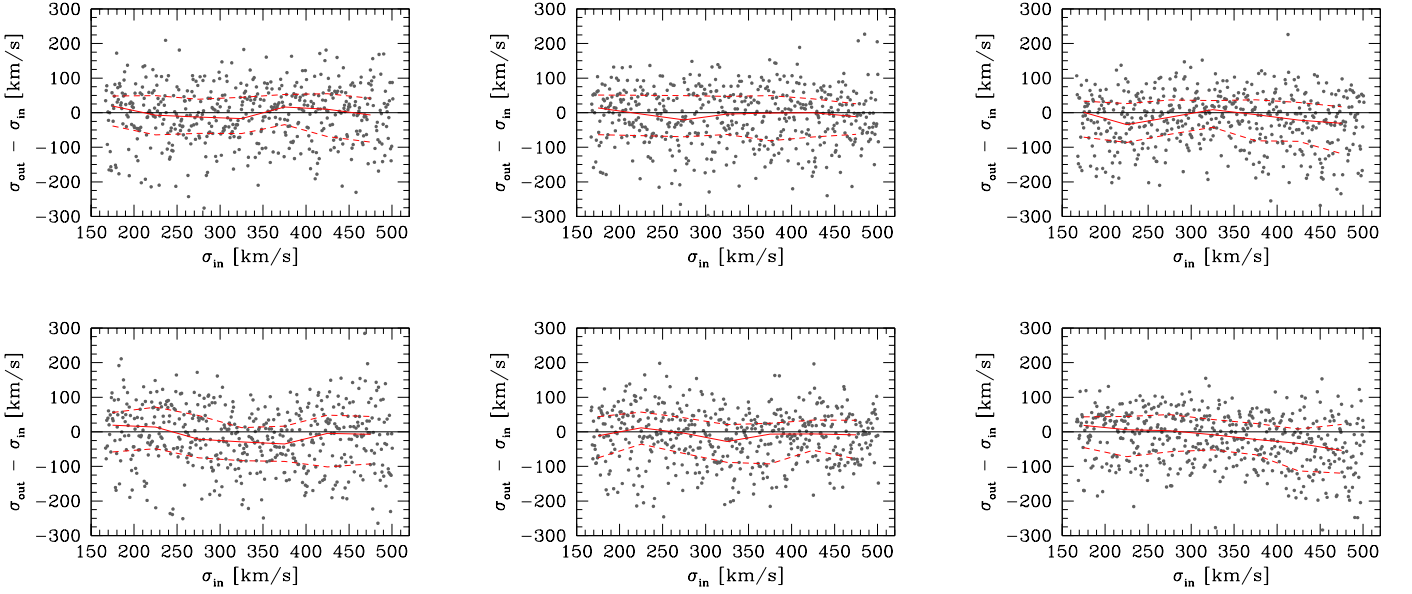


Fig. D.5. The same as Fig. D.2 for galaxy S2F1-389.

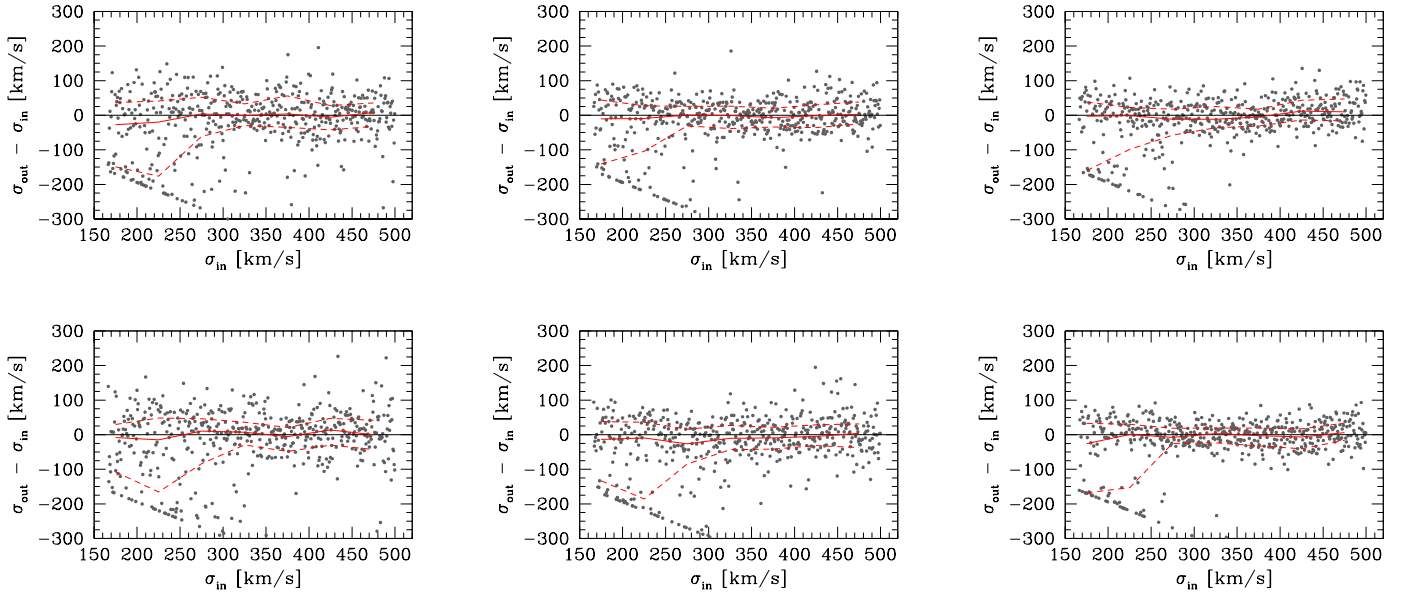


Fig. D.6. The same as Fig. D.2 for galaxy S2F1-443.